nature biotechnology

Brief Communication

https://doi.org/10.1038/s41587-025-02701-0

Identification of non-canonical peptides with moPepGen

Received: 27 March 2024

Accepted: 8 May 2025

Published online: 16 June 2025

Check for updates

Chenghao Zhu[1,2,3,4,8] ✉, Lydia Y. Liu[1,2,5,6,7,8], Annie Ha[5,6], Takafumi N. Yamaguchi[1,2,3], Helen Zhu[5,6,7], Rupert Hugh-White[1,2,3], Julie Livingstone[1,2,3], Yash Patel[1,2,3], Thomas Kislinger[5,6] ✉ & Paul C. Boutros[1,2,3,4,5] ✉

Proteogenomics is limited by the challenge of modeling the complexities of gene expression. We create moPepGen, a graph-based algorithm that comprehensively generates non-canonical peptides in linear time. moPepGen works with multiple technologies, in multiple species and on all types of genetic and transcriptomic data. In human cancer proteomes, it enumerates previously unobservable noncanonical peptides arising from germline and somatic genomic variants, noncoding open reading frames, RNA fusions and RNA circularization.

A single stretch of DNA can give rise to multiple protein products through genetic variation and through transcriptional, post-transcriptional and post-translational processes, such as RNA editing, alternative splicing and RNA circularization[1–4]. The number of potential proteoforms rises combinatorically with the number of possibilities at each level, so despite advances in proteomics technologies[5,6], much of the proteome is undetected in high-throughput studies[7].

The most common strategies to detect peptide sequences absent from canonical reference databases[7–9] (that is, non-canonical peptides; Supplementary Note 1), are de novo sequencing and open search. Despite continued algorithmic improvements, these strategies are computationally expensive, have elevated false-negative rates and lead to difficult data interpretation and variant identification issues[10,11]. As a result, the vast majority of proteogenomic studies use non-canonical peptide databases that have incorporated DNA and RNA alterations[7]. These databases are often generated using DNA and RNA sequencing of the same sample, and this improves error rates relative to community-based databases (for example, UniProt[12], neXtProt[13] and the Protein Mutant Database[14]) by focusing the search space[7,15].

This type of sample-specific proteogenomics relies on the ability to predict all potential protein products generated by the complexity of gene expression. Modeling transcription, translation and peptide cleavage to fully enumerate the combinatorial diversity of non-canonical peptides is computationally demanding. To simplify the search-space, existing methods have focused on generating peptides caused by individual variants or variant types[16–33], greatly increasing false negative rates and even potentially resulting in false-positive detections if the correct peptide is absent from the database (Extended Data Table 1). To fill this gap, we created a graph-based algorithm for the exhaustive elucidation of protein sequence variations and subsequent in silico non-canonical peptide generation. This method is moPepGen (multi-omics peptide generator; Fig. 1a).

moPepGen captures peptides that harbor any combination of small variants (for example, single-nucleotide polymorphisms (SNPs), small insertions and deletions (indels) and RNA editing sites) occurring on canonical coding transcripts, as well as on non-canonical transcript backbones resulting from novel open reading frames (ORFs), transcript fusion, alternative splicing and RNA circularization (Supplementary Fig. 1). It performs variant integration, in silico translation and peptide cleavage in a series of three graphs for every transcript, enabling systematic traversal across every variant combination (Methods and Extended Data Fig. 1a–d). All three reading frames are explicitly modeled for both canonical coding transcripts and non-canonical transcript backbones to efficiently capture frameshift variants and facilitate three-frame ORF search (Extended Data Fig. 2a). Alternative splicing events (for example, retained introns) and transcript fusions

[1]Department of Human Genetics, University of California, Los Angeles, Los Angeles, CA, USA. [2]Jonsson Comprehensive Cancer Center, University of California, Los Angeles, Los Angeles, CA, USA. [3]Institute for Precision Health, University of California, Los Angeles, Los Angeles, CA, USA. [4]Department of Urology, University of California, Los Angeles, Los Angeles, CA, USA. [5]Department of Medical Biophysics, University of Toronto, Toronto, Ontario, Canada. [6]Princess Margaret Cancer Centre, University Health Network, Toronto, Ontario, Canada. [7]Vector Institute for Artificial Intelligence, Toronto, Ontario, Canada. [8]These authors contributed equally: Chenghao Zhu, Lydia Y. Liu. ✉e-mail: chenghaozhu@mednet.ucla.edu; thomas.kislinger@utoronto.ca; pboutros@mednet.ucla.edu

https://doi.org/10.1038/s41587-025-02701-0

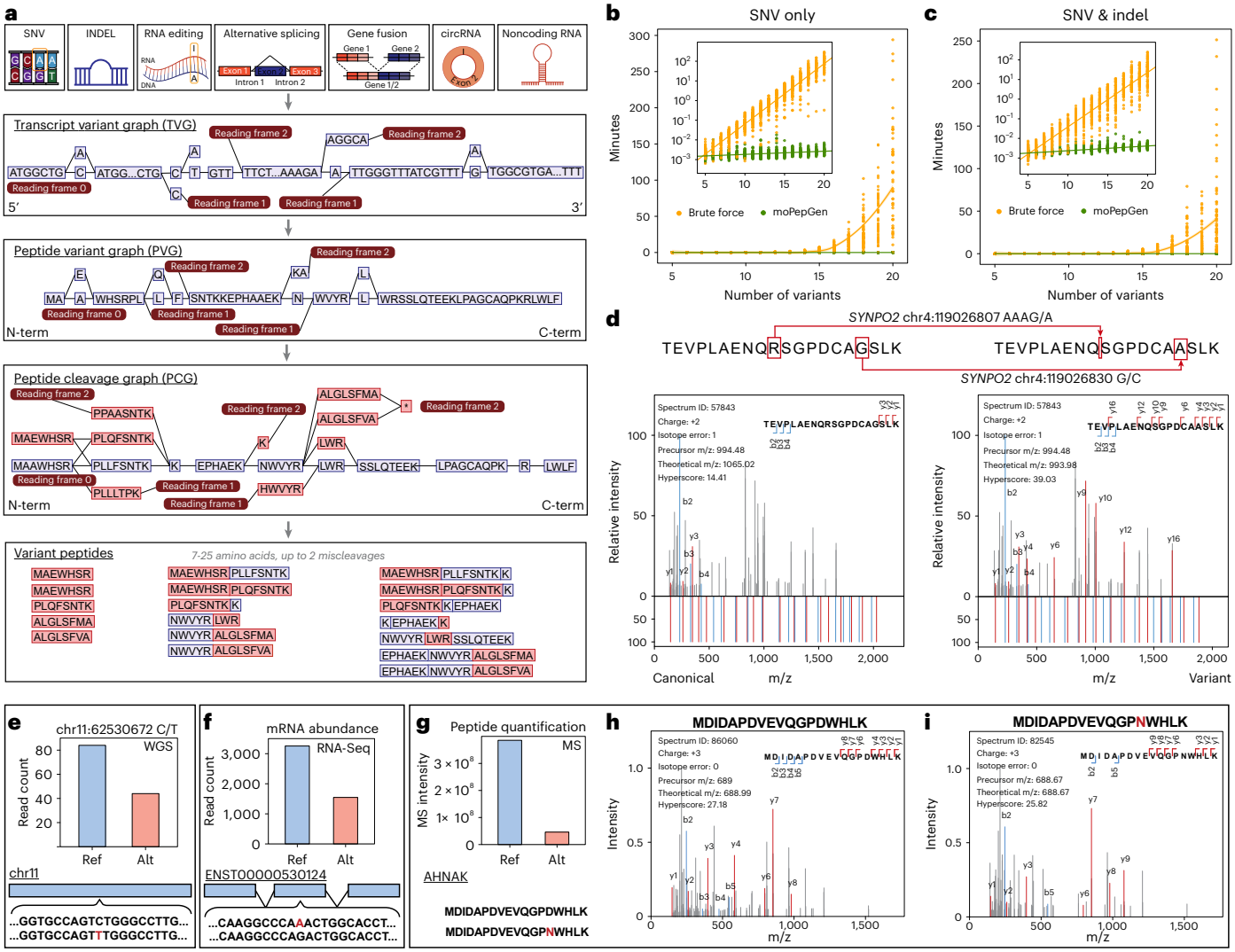

Fig. 1 | moPepGen is a graph-based algorithm that uncovers non-canonical peptides with variant combinations. a, moPepGen algorithm schematic. moPepGen is a graph-based algorithm that generates databases of non-canonical peptides that harbor genomic and transcriptomic variants (for example, single-nucleotide variant (SNV), small insertion and deletion (INDEL), RNA editing, alternative splicing, gene fusion and circular RNA (circRNA)) from coding transcripts, as well as from novel open reading frames of noncoding transcripts. C-term, C terminus; N-term, N terminus. **b**,**c**, moPepGen achieves linear runtime complexity when fuzz testing with SNVs only (**b**) and with SNVs and indels (**c**), based on 1,000 simulated test cases in each panel. **d**, A variant peptide from *SYNPO2* that harbors a small deletion and an SNV. Fragment ion mass spectrum from peptide-spectrum match (PSM) of the non-canonical peptide harboring two variants (top, both) is compared against the canonical peptide theoretical spectra (left, theoretical spectra at the bottom) and against the variant peptide theoretical spectra (right, bottom). Fragment ion matches are colored, with b-ions in blue and y-ions in red. **e**–**g**, A somatic SNV D1249N in *AHNAK* was detected in DNA sequencing of a prostate tumor (CPCG0183) at chr11:62530672 (**e**), in RNA sequencing (**f**) and as the non-canonical peptide MDIDAPDVEVQGP**N**WHLK (**g**). RNA-Seq, RNA sequencing; WGS, whole-genome sequencing. **h**,**i**, Fragment ion mass spectrum from PSM of the canonical peptide MDIDAPDVEVQGP**D**WHLK (**h**) and the non-canonical peptide (**i**). *m/z*, mass-to-charge ratio.

are modeled as subgraphs with additional small variants (Extended Data Fig. 2b). Graphs are replicated four times to fully cover peptides of back-splicing junction read-through in circular RNAs (circRNAs; Extended Data Fig. 2c,d). moPepGen outputs non-canonical peptides that cannot be produced by the chosen canonical proteome database. It documents all possible sources of each peptide to eliminate redundancy, such as where different combinations of genomic and transcriptomic events can produce the same non-canonical peptide.

We first validated moPepGen using 1,000,000 iterations of fuzz testing (Supplementary Fig. 2). For each iteration, a transcript model, its nucleotide sequence, and a set of variants composed of all supported variant types were simulated. Then non-canonical peptides generated by moPepGen were compared with those from a ground-truth brute-force algorithm. moPepGen demonstrated perfect accuracy and linear runtime complexity (4.7×10^{-3} seconds per variant) compared to exponential runtime complexity for the brute-force method (Fig. 1b,c). A comprehensive non-canonical peptide database of human germline polymorphisms was generated with 15 GB memory in 3.2 h on a 16-core compute node; the brute-force method was unable to complete this task.

Having established the accuracy of moPepGen, we next compared it to two popular custom database generators, customProDBJ[18] and pyQUILTS[22]. We tested all three methods on five prostate tumors with extensive multi-omics characterization[34–36]. We first evaluated the simple case of germline and somatic point mutations and indels. Most peptides (84.0 ± 0.9% (median ± median absolute deviation (MAD))) were predicted by all three methods, with moPepGen being modestly more sensitive (Extended Data Fig. 3a). Next, we considered the biological complexity of alternative splicing, RNA editing, RNA circularization and transcript fusion. Only moPepGen was able to evaluate peptides generated by all four of these processes, and therefore

80.2 ± 2.1% (median ± MAD) of peptides were uniquely predicted by moPepGen (Extended Data Fig. 3b). By contrast only 3.2% of peptides were not predicted by moPepGen, and these corresponded to specific assumptions around the biology of transcription and translation made by other methods (Extended Data Fig. 3c and Methods). By generating a more comprehensive database, moPepGen enabled the unique detection of 53.7 ± 12.2% (median ± MAD) peptides from matched proteomic data (Extended Data Fig. 3d). An example of a complex variant peptide identified only by moPepGen is the combination of a germline in-frame deletion followed by a substitution in *SYNPO2* (Fig. 1d). In addition, moPepGen's clear variant annotation system readily enables peptide verification across the central dogma. For example, the somatic mutation D1249N in *AHNAK* was detected in ~30% of both DNA and RNA reads and was detected by mass spectrometry (MS; Fig. 1e–i), confirmed by three search engines. Taken together, these benchmarking results demonstrate the robust and comprehensive nature of moPepGen.

To illustrate the use of moPepGen for proteogenomic studies, we first evaluated it across multiple proteases (Extended Data Fig. 4a). Using independent conservative control of false discovery rate (FDR) across canonical and custom databases (Methods and Supplementary Fig. 3)[7,18], we focused on detection of novel ORFs (that is, polypeptides from transcripts canonically annotated as noncoding) across seven proteases[37] in a deeply fractionated human tonsil sample[38] (Supplementary Table 1). moPepGen enabled the detection of peptides from 1,787 distinct ORFs previously thought to be noncoding, and these peptides were most easily detected with the Arg-C protease (Extended Data Fig. 4b), suggesting alternative proteases may enhance noncoding ORF detection (Extended Data Fig. 4c). In total, 184 noncoding ORFs were detected across four or more proteomic preparation methods in this single sample, demonstrating that moPepGen can reliably identify novel proteins (Extended Data Fig. 4d,e).

We next sought to demonstrate that moPepGen can benefit analyses in different species by studying germline variation in the C57BL/6 N mouse[37,39]. Using strain-specific germline SNPs and indels from the Mouse Genome Project[37,39], moPepGen predicted 5,481 non-canonical peptides arising from variants in protein-coding genes and 15,475 peptides from noncoding transcript novel ORFs (Extended Data Fig. 5a). Across the proteomes of three bulk tissues (cerebellum, liver and uterus), we detected 18 non-canonical peptides in protein-coding genes and 343 from noncoding ORFs (Extended Data Fig. 5b–d and Supplementary Table 2). Thus, moPepGen can support proteogenomics in non-human studies to identify variants of protein-coding genes and novel proteins.

To evaluate the use of moPepGen for somatic variation, we analyzed 375 human cancer cell line proteomes with matched somatic mutations and transcript fusions[40,41] (Supplementary Data). moPepGen processed each cell line in 2:58 min (median ± 1:20 min, MAD), generating 2,683 ± 2,513 (median ± MAD) potential non-canonical variant peptides per cell line. The number of predicted variant peptides varied strongly with tissue of origin, ranging from median of 838 to 16,255 (Fig. 2a), and was driven largely by somatic mutations in protein-coding genes and by fusion events in noncoding genes (Extended Data Fig. 6a–c). Searching the cell line proteomes identified 39 ± 27 (median ± MAD) non-canonical peptides per cell line (Methods and Supplementary Fig. 4). The majority of these were derived from noncoding transcript ORFs (Extended Data Fig. 6d and Supplementary Table 3). Variant peptides from coding somatic mutations were more easily detected than those from transcript fusion events (Extended Data Fig. 6e,f). A total of 26 genes had variant peptides detected in cell lines from three or more tissues of origin, including the cancer driver genes *TP53*, *KRAS* and *HRAS* (Fig. 2b). Peptide evidence was also found for fusion transcripts involving cancer driver genes like *MET* and *STK11* (Extended Data Fig. 6g,h). We validated non-canonical peptide-spectrum matches (PSMs) by predicting tandem mass (MS2) spectra using Prosit[42] and verifying that variant peptide MS2 spectra correlated better with predictions based on the matched non-canonical peptide sequences than predictions based on their canonical peptide counterparts (Methods and Extended Data Fig. 6i). Coding variant peptide PSMs also showed high cross-correlations with their Prosit-predicted variant MS2 spectra, on par with those of canonical PSMs and their canonical spectra (Extended Data Fig. 6j). Thus, moPepGen can effectively and rapidly detect variant peptides arising from somatic variation. These variant peptides may also prove to harbor functional consequences in future studies. Genes, such as *KRAS*, trended toward greater essentiality for cell growth in multiple cell lines with non-canonical peptide hits, and the effects may be independent of gene dosage (Extended Data Fig. 7a–c). Across cell lines, detected variant peptides were also predicted to give rise to 416 putative neoantigens (3.0 ± 1.5, median ± MAD per cell line; Extended Data Fig. 7d and Supplementary Table 4), including recurrent neoantigens in *KRAS*, *TP53* and *FUBP3* (Extended Data Fig. 7e).

We next sought to demonstrate the use of moPepGen in data-independent acquisition (DIA) MS using eight clear cell renal cell carcinoma tumors with matched whole-exome sequencing, RNA sequencing and DIA proteomics[43]. In each tumor, moPepGen predicted 157,016 ± 34,215 (median ± MAD) unique variant peptides from protein-coding genes (Extended Data Fig. 8a). Using a Prosit-generated spectral library, we detected 307 ± 112 (median ± MAD) variant peptides in each tumor using DIA-NN[44] (Extended Data Fig. 8b and Supplementary Table 5). Germline-SNP and alternative splicing were the most common sources of detected variant peptides (Extended Data Fig. 8c,d). Non-canonical peptides derived from RNA editing events were detected in 21 genes (Extended Data Fig. 8e–i). Thus, moPepGen can enable the detection of variant peptides from DIA proteomics.

Finally, to demonstrate the use of moPepGen on complex and comprehensive gene expression data, we analyzed five primary prostate cancer samples with matched DNA whole-genome sequencing, ultra-deep ribosomal-RNA-depleted RNA sequencing and MS-based proteomics[34–36]. moPepGen generated 1,382,666 ± 64,281 (median ± MAD) unique variant peptides per sample, spanning 115 variant combination categories (Fig. 2c). Searching this database resulted in the detection of 206 ± 56 (median ± MAD) non-canonical peptides per sample, with 138 ± 28 (median ± MAD) derived from protein-coding genes (Extended Data Fig. 9a and Supplementary Table 6). The distribution of intensities and Comet expectation scores of non-canonical PSMs closely resembled that of canonical PSMs and was distinct from all decoy hits (Supplementary Fig. 5), lending confidence in our non-canonical peptide detection. All samples harbored proteins containing multiple variant peptides (9 ± 1.5, median ± MAD proteins per tumor; range 2–6 variant peptides per protein; Fig. 2d). Some detected peptides harbored multiple variants, including two from prostate-specific antigen (PSA from the *KLK3* gene; Extended Data Fig. 9b). Germline SNPs were the major common cause of variant peptides on coding transcripts and alternative splicing events were the most common cause on noncoding transcripts (Extended Data Fig. 9c–e). Nine genes showed recurrent detection of peptides caused by circRNA back-splicing (Extended Data Fig. 9f–g), with 36/78 circRNA PSMs validated by de novo sequencing (Supplementary Table 7)[45]. These recurrent circRNA-derived peptides were verified in five additional prostate tumors (Supplementary Fig. 6). We also detected four peptides from noncoding transcripts with the recently reported tryptophan-to-phenylalanine substitutants[46]. Thus, moPepGen can identify peptides resulting from highly complex layers of gene expression regulation.

moPepGen is a computationally efficient algorithm that enumerates transcriptome and proteome diversity across arbitrary variant types. It enables the detection of variant and novel ORF peptides across species, proteases and technologies. moPepGen integrates into existing proteomic analysis workflows, and can broadly enhance proteogenomic analyses for many applications.

https://doi.org/10.1038/s41587-025-02701-0

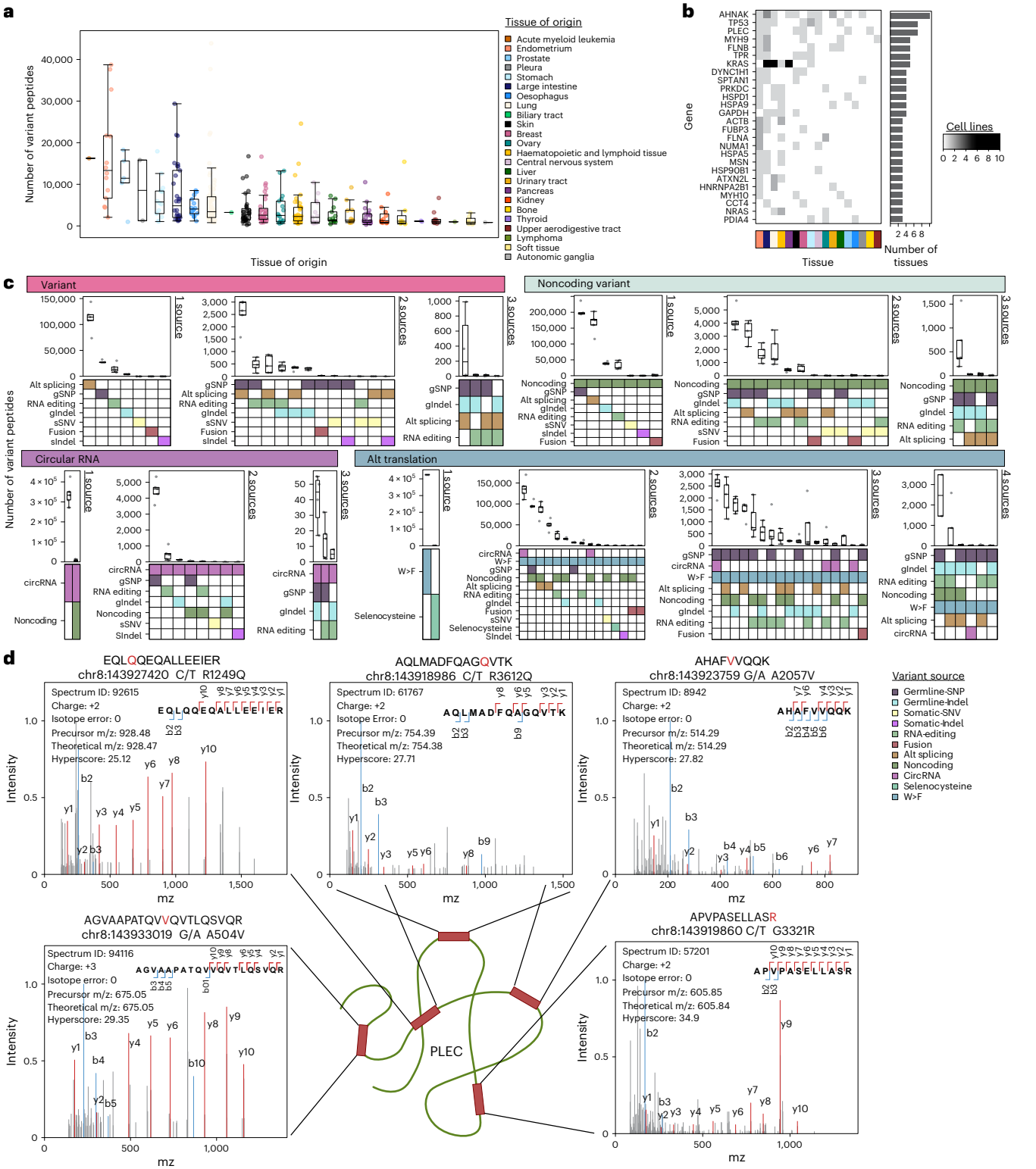

Fig. 2 | moPepGen generates comprehensive non-canonical databases that support proteogenomic analysis. a, Sizes of variant peptide databases generated by moPepGen using somatic SNVs, small insertions and deletions and transcript fusions for 376 cell lines from the Cancer Cell Line Encyclopedia project. Color indicates cell line tissue of origin. The number of cell lines per tissue of origin is provided in Supplementary Table 8. **b**, Genes with variant peptides detected in cell lines across three or more tissues of origin (bottom covariate). The barplot shows number of recurrences across tissues and color of heatmap indicates number of cell lines. **c**, Number of non-canonical peptides from different variant combinations (bottom heatmap) generated using genomic and transcriptomic data from five primary prostate tumors ($n = 5$), shown across four tiers of custom databases and grouped by the number of variant sources in combination. Alternative translation (Alt Translation) sources with ≥10 peptides are visualized. gSNP, germline SNP; gIndel, germline small insertion and deletion (indel); sSNV, somatic single-nucleotide variant; sIndel, somatic indel; W > F: tryptophan-to-phenylalanine. **d**, Five variant peptides detected in one prostate tumor (CPCG0183) from the protein plectin (PLEC). Fragment ion matches are colored, with b-ions in blue and y-ions in red. *m/z*, mass-to-charge ratio. All boxplots show the first quartile, median, to the third quartile, with whiskers extending to furthest points within 1.5× the interquartile range.

Online content

Any methods, additional references, Nature Portfolio reporting summaries, source data, extended data, supplementary information, acknowledgements, peer review information; details of author contributions and competing interests; and statements of data and code availability are available at https://doi.org/10.1038/s41587-025-02701-0.

References

1. Zhang, B. et al. Proteogenomic characterization of human colon and rectal cancer. *Nature* **513**, 382–387 (2014).
2. Sinitcyn, P. et al. Global detection of human variants and isoforms by deep proteome sequencing. *Nat. Biotechnol.* **41**, 1776–1786 (2023).
3. Nilsen, T. W. & Graveley, B. R. Expansion of the eukaryotic proteome by alternative splicing. *Nature* **463**, 457–463 (2010).
4. Peng, X. et al. A-to-I RNA editing contributes to proteomic diversity in cancer. *Cancer Cell* **33**, 817–828.e7 (2018).
5. Creighton, C. J. Clinical proteomics towards multiomics in cancer. *Mass Spectrom. Rev.* https://doi.org/10.1002/MAS.21827 (2022).
6. Edwards, N. J. et al. The CPTAC data portal: a resource for cancer proteomics research. *J. Proteome Res.* **14**, 2707–2713 (2015).
7. Nesvizhskii, A. I. Proteogenomics: concepts, applications and computational strategies. *Nat. Methods* **11**, 1114–1125 (2014).
8. Chick, J. M. et al. A mass-tolerant database search identifies a large proportion of unassigned spectra in shotgun proteomics as modified peptides. *Nat. Biotechnol.* **33**, 743–749 (2015).
9. Rodriguez, H., Zenklusen, J. C., Staudt, L. M., Doroshow, J. H. & Lowy, D. R. The next horizon in precision oncology: proteogenomics to inform cancer diagnosis and treatment. *Cell* **184**, 1661–1670 (2021).
10. Ma, B. & Johnson, R. De novo sequencing and homology searching. *Mol. Cell Proteomics* **11**, O111.014902 (2012).
11. Fu, Y. Data analysis strategies for protein modification identification. *Methods Mol. Biol.* **1362**, 265–275 (2016).
12. Bateman, A. UniProt: a worldwide hub of protein knowledge. *Nucleic Acids Res.* **47**, D506–D515 (2019).
13. Lane, L. et al. neXtProt: a knowledge platform for human proteins. *Nucleic Acids Res.* **40**, D76–D83 (2012).
14. Kawabata, T., Ota, M. & Nishikawa, K. The Protein Mutant Database. *Nucleic Acids Res.* **27**, 355–357 (1999).
15. Salz, R. et al. Personalized proteome: comparing proteogenomics and open variant search approaches for single amino acid variant detection. *J. Proteome Res* **20**, 3353–3364 (2021).
16. Wang, X. et al. Protein identification using customized protein sequence databases derived from RNA-seq data. *J. Proteome Res* **11**, 1009–1017 (2012).
17. Wang, X., Zhang, B. & Wren, J. customProDB: an R package to generate customized protein databases from RNA-seq data for proteomics search. *Bioinformatics* **29**, 3235–3237 (2013).
18. Wen, B., Li, K., Zhang, Y. & Zhang, B. Cancer neoantigen prioritization through sensitive and reliable proteogenomics analysis. *Nat. Commun.* **11**, 1–14 (2020). *2020 11:1*.
19. Sinitcyn, P., Gerwien, M. & Cox, J. MaxQuant module for the identification of genomic variants propagated into peptides. *Methods Mol. Biol.* **2456**, 339–347 (2022).
20. Van De Geer, W. S., Van Riet, J. & Van De Werken, H. J. G. ProteoDisco: a flexible R approach to generate customized protein databases for extended search space of novel and variant proteins in proteogenomic studies. *Bioinformatics* **38**, 1437–1439 (2022).
21. Umer, H. M. et al. Generation of ENSEMBL-based proteogenomics databases boosts the identification of non-canonical peptides. *Bioinformatics* **38**, 1470–1472 (2022).
22. Ruggles, K. V. et al. An analysis of the sensitivity of proteogenomic mapping of somatic mutations and novel splicing events in cancer. *Mol. Cell. Proteom.* **15**, 1060–1071 (2016).
23. Sheynkman, G. M., Shortreed, M. R., Frey, B. L. & Smith, L. M. Discovery and mass spectrometric analysis of novel splice-junction peptides using RNA-seq. *Mol. Cell. Proteom.* **12**, 2341–2353 (2013).
24. Sheynkman, G. M. et al. Using Galaxy-P to leverage RNA-Seq for the discovery of novel protein variations. *BMC Genomics* **15**, 1–9 (2014).
25. Sheynkman, G. M., Shortreed, M. R., Frey, B. L., Scalf, M. & Smith, L. M. Large-scale mass spectrometric detection of variant peptides resulting from nonsynonymous nucleotide differences. *J. Proteome Res* **13**, 228–240 (2014).
26. Wen, B. et al. sapFinder: an R/Bioconductor package for detection of variant peptides in shotgun proteomics experiments. *Bioinformatics* **30**, 3136–3138 (2014).
27. Wen, B. et al. PGA: an R/Bioconductor package for identification of novel peptides using a customized database derived from RNA-Seq. *BMC Bioinformatics* **17**, 1–6 (2016).
28. Woo, S. et al. Proteogenomic database construction driven from large scale RNA-seq data. *J. Proteome Res.* **13**, 21–28 (2014).
29. Woo, S. et al. Proteogenomic strategies for identification of aberrant cancer peptides using large-scale next-generation sequencing data. *Proteomics* **14**, 2719–2730 (2014).
30. Cesnik, A. J. et al. Spritz: a proteogenomic database engine. *J. Proteome Res.* **20**, 1826–1834 (2021).
31. Cifani, P. et al. ProteomeGenerator: a framework for comprehensive proteomics based on de novo transcriptome assembly and high-accuracy peptide mass spectral matching. *J. Proteome Res.* **17**, 3681–3692 (2018).
32. Huber, F. et al. A comprehensive proteogenomic pipeline for neoantigen discovery to advance personalized cancer immunotherapy. *Nat. Biotechnol.* https://doi.org/10.1038/s41587-024-02420-y (2024).
33. Kwok, N. et al. Integrative proteogenomics using ProteomeGenerator2. *J. Proteome Res.* **22**, 2750–2764 (2023).
34. Chen, S. et al. Widespread and functional RNA circularization in localized prostate cancer. *Cell* **176**, 831–843.e22 (2019).
35. Fraser, M. et al. Genomic hallmarks of localized, non-indolent prostate cancer. *Nature* **541**, 359–364 (2017).
36. Sinha, A. et al. The Proteogenomic Landscape of Curable Prostate Cancer. *Cancer Cell* **35**, 414–427.e6 (2019).
37. Giansanti, P. et al. Mass spectrometry-based draft of the mouse proteome. *Nat. Methods* **19**, 803–811 (2022).
38. Wang, D. et al. A deep proteome and transcriptome abundance atlas of 29 healthy human tissues. *Mol. Syst. Biol.* **15**, e8503 (2019).
39. Keane, T. M. et al. Mouse genomic variation and its effect on phenotypes and gene regulation. *Nature* **477**, 289–294 (2011).
40. Ghandi, M. et al. Next-generation characterization of the Cancer Cell Line Encyclopedia. *Nature* **569**, 503–508 (2019).
41. Nusinow, D. P. et al. Quantitative Proteomics of the Cancer Cell Line Encyclopedia. *Cell* **180**, 387–402.e16 (2020).
42. Gessulat, S. et al. Prosit: proteome-wide prediction of peptide tandem mass spectra by deep learning. *Nat. Methods* **16**, 509–518 (2019). *2019 16:6*.
43. Li, Y. et al. Histopathologic and proteogenomic heterogeneity reveals features of clear cell renal cell carcinoma aggressiveness. *Cancer Cell* **41**, 139–163.e17 (2023).
44. Demichev, V., Messner, C. B., Vernardis, S. I., Lilley, K. S. & Ralser, M. DIA-NN: neural networks and interference correction enable deep proteome coverage in high throughput. *Nat. Methods* **17**, 41–44 (2020).
45. Ma, B. Novor: real-time peptide de novo sequencing software. *J. Am. Soc. Mass. Spectrom.* **26**, 1885–1894 (2015).
46. Pataskar, A. et al. Tryptophan depletion results in tryptophan-to-phenylalanine substitutants. *Nature* **603**, 721–727 (2022). *2022 603:7902*.

https://doi.org/10.1038/s41587-025-02701-0

https://doi.org/10.1038/s41587-025-02701-0

Methods

Transcript Variant Graph

A transcript variant graph (TVG) is instantiated for each transcript, incorporating all associated variants. In a TVG, nodes are transcript fragments with reference or alternative nucleotide sequences, whereas edges are the opening or closing of variant nodes connecting them to the reference sequence, or the elongation of reference sequences. The TVG starts with three linear nodes of the entire transcript sequence representing the three reading frames, offset by 0, 1 or 2 nucleotides from the transcript 5′ end. A variant is incorporated into the graph by breaking the node at the variant's start and end positions and attaching a new node with the alternative sequence to the new upstream and downstream nodes. An in-frame variant is represented as a node with incoming and outgoing nodes in the same reading frame subgraph, whereas frameshifting variants have incoming nodes and outgoing nodes in different reading frames. The outgoing reading frame index equals to $(S_{ref}–S_{alt})$ *mod* 3, where S_{ref} is the length of the reference sequence and S_{alt} is the length of the alternative sequence. For transcripts with an annotated known canonical ORF, variants are only incorporated into the subgraph of the appropriate reading frame (Extended Data Fig. 2a). If frameshifting variants are present, downstream variants are also incorporated into the subgraphs of the outgoing frameshift nodes. For transcripts without an annotated ORF, all variants are incorporated into all three reading frames (Extended Data Fig. 2a). Large insertions and substitutions as the result of alternative splicing events (for example, retained introns, alternative 3′/5′ splicing, *etc*.) are represented as subgraphs that can carry additional variants (Extended Data Fig. 2b).

Variant bubbles and peptide variant graph

After the TVG has been populated with all variants, nodes that overlap with each other in transcriptional coordinates are aligned to create variant bubbles within which all nodes point to the same upstream and downstream nodes (Extended Data Fig. 1b). This is done by first finding connection nodes in the TVG, the reference nodes without any variants that connect two variant bubbles after they are aligned. The root node is the first connection node, and the next connection node is found by looking for the first commonly connected downstream node with length of five or more nucleotides that is outbound to more than one node (Supplementary Note 2 and Supplementary Fig. 7). Nodes between the two connection nodes are then aligned to form a variant bubble by generating all combinations of merged nodes so that they all point to the same upstream and downstream nodes (Extended Data Fig. 1b). Overlapping variants in the variant bubble are automatically eliminated because they are disjoint. The sequence lengths of nodes in the variant bubble are also adjusted by taking nucleotides from the commonly connected upstream and downstream nodes to ensure that they are multiples of three. A peptide variant graph (PVG) is then instantiated by translating the nucleotide sequence of each TVG node into amino acid sequences.

Peptide cleavage graph

A PVG is converted into a peptide cleavage graph (PCG), where each edge represents an enzymatic cleavage site (Extended Data Fig. 1c). For connection nodes, all enzymatic cleavage sites are first identified, and the node is cleaved at each cleavage site. Because enzymatic cleavage site motifs can span over multiple nodes (for example, the trypsin exception of not cutting given K/P but cutting given WK/P), connection nodes are also merged with each downstream and/or upstream node and cut at additional cleavage sites if found. To optimize run time, different merge-and-cleave operations are used depending on the number of incoming and outgoing nodes, and the number of cleavage sites in a node (Supplementary Fig. 8). Hypermutated regions where variant bubbles contain many variants and/or the lack of cleavage sites in connection nodes can result in an exponential increase in the number of nodes in the aligned variant bubble. We use a pop-and-collapse strategy, such that when merge-and-cleave is applied to a connection node, x number of amino acids are popped from the end of each node in the variant bubble. The popped nodes are collapsed if they share the same sequence. The pop-and-collapse operation is only applied when the number of nodes in a variant bubble exceeds a user-defined cutoff.

Calling variant peptides

Variant peptides with the permitted number of miscleavages are called by traversing through the PCG. We use a stage-and-call approach that first visits all incoming nodes to determine the valid ORFs of a peptide node (Supplementary Note 3). Stage-and-call also allows cleavage-gain mutations and upstream frameshift mutations to be carried over to the downstream peptide nodes. Peptide nodes are then extended by merging with downstream nodes to call variant peptides with miscleavages (Supplementary Note 4). For noncoding transcripts, novel ORF start sites, including those caused by start-gain mutations, are found by looking for any methionine (M) in all three subgraphs. Terminology used in subsequent sections, including canonical and non-canonical database, variant peptides, non-canonical peptides and proteoform, is defined in Supplementary Note 1.

Fusion and circular transcripts

Most fusion transcript callers detect fusion events between genes, causing ambiguity of which transcripts of the genes are involved in a particular fusion event. We took the most comprehensive approach and endeavored to capture all possible variant peptides by assuming that a fusion event could happen between any transcript of the donor and accepter genes. Fusion transcripts are considered as novel backbones in graph instantiation, with an individual graph instantiated for each donor and acceptor transcript pair. Single-nucleotide variants (SNVs) and small insertion/deletions (indels) of both donor and acceptor transcripts are incorporated into the TVG. The translated and cleaved PCG is then traversed to call variant peptides, identical to a canonical transcript backbone. If the fusion breakpoint occurs in an intron, the intronic nucleotide sequence leading up to or following the breakpoint is retained as unspliced, and its associated intronic variants are included. The ORF start site of the donor transcript is used if exists when calling variant peptides. The fusion transcript is treated as a noncoding transcript if the donor transcript is annotated as noncoding.

Similar to fusion transcripts, circRNAs are treated as novel backbones, with an individual graph instantiated for each circRNA (Extended Data Fig. 2c). A circular variant graph (a counterpart to TVG) is instantiated by connecting the linear sequence of the circRNA onto itself at the back-splice junction and incorporating SNVs and indels. Novel peptides can theoretically be translated from circRNAs if a start codon is present, by ribosome read-through across the back-splicing junction site. If the circRNA length is not a multiple of three nucleotides, translation across the back-splicing site induces a frameshift. Without a stop codon, the ribosome may traverse the circRNA up to three times before the amino acid sequence repeats. Therefore, moPepGen extends the circular graph linearly by appending three copies of each reading frame as a subgraph to account for frameshifts. The extended graph is then translated to a PVG and converted to a PCG. Variant peptides are called by treating every circRNA as a noncoding transcript and scanning all novel start codons in all three reading frames.

Biological assumptions for edge cases

moPepGen applies various assumptions to selectively include or exclude certain variant events or peptides (Extended Data Fig. 3c). Start-codon-altering variants are excluded due to the uncertainty around whether and where translation will still occur. Similarly, splice-site-altering variants are omitted due to the complexity of splicing determinants, which can result in skipping to the next canonical or non-canonical splice site. We terminate translation at the last complete peptide when stop codons are unknown, as incomplete transcript

annotations create ambiguity in downstream sequences, obscuring enzymatic cleavage sites. Stop-codon-altering variants do not extend translation beyond the transcript, as the downstream genomic region is not assumed to be part of the RNA transcript.

GVF file format and parsers

Genomic (SNPs, SNVs, indels) and transcriptomic variants (fusion transcripts, RNA editing sites, alternative splicing transcripts, circRNAs) are first converted into gene-centric entries for each transcript that they impact. We defined a gene-based GVF (genetic variant format) derived from VCF (variant calling format) to store all relevant information for each variant, including the gene ID and offset. moPepGen includes built-in parsers to convert variant caller outputs into GVFs. SNPs, SNVs and indels require the annotation via Variant Effect Predictor (VEP)[47] for compatibility with the parseVEP module. Parsers for fusion, alternative splicing, RNA editing and circRNA operate directly on native outputs. moPepGen is implemented in Python and supports easy extension and addition of new parsers. The full Nextflow pipeline (https://github.com/uclahs-cds/pipeline-call-NonCanonicalPeptide)[48,49,50], automates data preprocessing, peptide prediction and database tiering, with optional transcript abundance filtering. Our DNA data processing pipeline is described elsewhere[51].

Fuzz testing and brute force algorithm

To validate moPepGen, we implemented a fuzz testing framework where transcripts with varying properties (for example, coding status, strand, selenocysteine and start or stop codon position) and artificial sequences are simulated. Each is paired with simulated variants across all supported types. The resulting peptides are compared against those generated by a brute force algorithm, which iterates through all possible variant combinations to identify non-canonical peptides. The brute force algorithm also performs three-frame translation for noncoding transcripts. Fuzz testing and the brute force algorithm are included in the moPepGen package.

Datasets

Cancer Cell Line Encyclopedia proteome. Proteomic characterization of 375 cell lines from the Cancer Cell Line Encyclopedia (CCLE) was obtained from Nusinow et al.[41]. Fractionated raw mass spectrometry (MS) data were downloaded from MassIVE (project ID: MSV000085836). Somatic SNVs and indels, and fusion transcript calls were downloaded from the DepMap portal (https://depmap.org/portal, 22Q1). Somatic SNVs and indels were converted to GRCh38 coordinates from hg19 using CrossMap (v0.5.2)[52]. Gene and transcript IDs were assigned to each SNV/indel using VEP (v104)[53] with genomic annotation GTF downloaded from GENCODE (v34)[54]. Fusion results were aligned to the GENCODE v34 reference by first lifting over the fusion coordinates to GRCh38 using CrossMap (v0.5.2). After liftover, the records were removed if the donor or acceptor breakpoint location was no longer associated with the gene, if either breakpoint dinucleotides did not match with the reference or if either gene ID was not present in GENCODE (v34).

Mouse proteome. MS-based proteome of mouse strain C57BL/6 N was obtained from Giansanti et al.[37]. Fractionated raw MS data of the liver, uterus and cerebellum proteomes were downloaded from the PRIDE repository (project ID: PXD030983). Germline SNPs and indels were obtained from the Mouse Genomes Project[39] with GRCm38 VCFs downloaded from the European Variation Archive (accession: PRJEB43298). Germline SNPs and indels were annotated using VEP (v102) against Ensembl GRCm38 (v102)[47].

Alternative protease and fragmentation proteome. A human tonsil tissue processed using ten different combinations of proteases and peptide fragmentation methods (ArgC_HCD, AspN_HCD, Chymotrypsin_CID, Chymotrypsin_HCD, GluC_HCD, LysC_HCD, LysN_HCD, Trypsin_CID, Trypsin_ETD, Trypsin_HCD) was obtained from Wang et al.[38]. Fractionated raw mass spectrometry data were downloaded from the PRIDE repository (project ID: PXD010154).

DIA proteome. DIA proteomic data from eight clear cell renal cell carcinoma (ccRCC) samples were obtained from Li et al.[43]. Raw mass spectrometry data were retrieved from the Proteomic Data Commons (PDC, PDC000411). WXS and RNA-seq BAM files were obtained from Genomic Data Commons (GDC, Project: CPTAC-3, Primary Site: Kidney). WXS data was processed using a standardized pipeline to identify germline SNPs, somatic SNVs and indels[51]. BAM files were reverted to FASTQ using Picard toolkit (v2.27.4) and SAMtools (v1.15.1)[55], realigned to GRCh38 using BWA-MEM2 (v2.2.1)[56], and calibrated using BQSR and IndelRealignment from GATK (v4.2.4.1)[57]. Germline SNPs and indels were called following GATK (v4.2.4.1) best practices[57,58], whereas somatic SNVs and indels were called using Mutect2 (from GATK v4.5.0.0), followed by annotation with VEP (v104)[53] against GENCODE v34. RNA-seq BAM files were converted to FASTQ using Picard toolkit (v2.27.4) and SAMtools (v1.15.1) and re-aligned to GRCh38.p13 with GENCODE v34 GTF using STAR (2.7.10b)[59]. Transcript fusion events were called using STAR-Fusion (v1.9.1)[60], alternative splicing events were called using rMATS (v4.1.1)[61] and RNA editing sites were called using REDItools2 (v1.0.0)[62] using paired RNA and DNA BAMs.

Prostate cancer proteome. The proteomic characterization of five prostate cancer tissues were obtained from Sinha et al.[36]. Raw mass spectrometry data were downloaded from MassIVE (project ID: MSV000081552). Germline SNPs and indels, as well as somatic SNVs and indels, were obtained from the ICGC Data Portal (Project code: PRAD-CA). Variants were indexed using VCFtools (v0.1.16)[63] and converted to GRCh38 using Picard toolkit (v2.19.0), followed by chromosome name mapping from the Ensembl to the GENCODE system using BCFtools (v1.9-1)[55]. Mutations were annotated using VEP (v104)[53] against GENCODE (v34). Raw mRNA sequencing data were obtained from Gene Expression Omnibus (accession: GSE84043). Transcriptome alignment was performed using STAR (v2.7.2) to reference genome GRCh38.p13 with GENCODE (v34) GTF and junctions were identified by setting the parameter–chimSegmentMin 10 (ref. 59). CIRCexplorer2 (v.2.3.8) was used to parse and annotate junctions for circRNA detection[64]. Fusion transcripts were called using STAR-Fusion (v1.9.1)[60]. RNA editing sites were called using REDItools2 using paired RNA and DNA BAMs (v1.0.0)[62]. Alternative splicing transcripts were called using rMATS (v4.1.1)[61].

Canonical database search

All MS raw files (.raw) were converted to mzML using ProteoWizard (3.0.21258)[65]. The GRCh38 human and the GRCm38 mouse canonical proteome databases were obtained from GENCODE (v34) and Ensembl (v102), respectively, with common contaminants[66] added and reversed sequences appended for target-decoy FDR control. Database searches were performed using Comet (v2019.01r5)[67] with static modifications of cysteine carbamidomethylation, and up to three variable modifications (methionine oxidation, protein N-terminus acetylation, peptide N-terminus pyroglutamate formation), under full trypsin digestion with up to two miscleavages (except for the tonsil samples processed with alternative enzymes), for peptide lengths 7–35. For CCLE, static modification of tandem mass tag (TMT; 10plex) on the peptide N-terminus and lysine residues and variable modification of TMT on serine residues were additionally included, following the original study. CCLE data were searched in low resolution with 20 ppm precursor mass tolerance, 0.5025 Da fragment mass tolerance, and clear TMT *m/z* range, following the original publication. All other datasets used high-resolution label-free quantification, with precursor mass tolerance of 20 ppm (mouse), 10 ppm (tonsil) and 30 ppm (prostate), and

fragment mass tolerance of 0.025 Da for tonsil or 0.01 Da otherwise, following original publications. Tonsil proteomes were searched with the appropriate fragmentation method setting and with the protease used in sample preparation, with a maximum of two miscleavages for Lys-C and Arg-C, three miscleavages for Glu-C and Asp-N and four miscleavages for chymotrypsin, as in the original publication[38]. The eight DIA ccRCC proteomes were not searched against a canonical database.

Peptide-level target-decoy FDR calculation was performed using the FalseDiscoveryRate module from OpenMS (v3.0.0-1f903c0)[68] using the formula (D + 1)/(T + D), where D and T are the numbers of decoy and target PSMs, respectively. Peptides were filtered at 1% FDR, and PSMs were removed from the corresponding mzML for subsequent non-canonical database search. Post hoc cohort-level FDR was calculated to verify an FDR cutoff smaller than 1%. Peptide quantification was performed using OpenMS FeatureFinderIdentification (v3.0.0-1f903c0)[69] with 'internal IDs only' and adjusted precursor mass tolerances as above, and otherwise default parameters. TMT quantification was performed using OpenMS IsobaricAnalyzer (v3.0.0-1f903c0), without isotope correction due to absence of correction matrix.

Non-canonical database generation

Human (GRCh38) and mouse (GRCm38) reference proteomes were obtained from GENCODE (v34) and Ensembl (v102), respectively. Non-canonical peptide databases were generated with trypsin digestion of up to two miscleavages and peptide lengths 7-25, except for alternative protease samples. Alternative translation peptides were generated using *callAltTranslation*, including those with selenocysteine termination[70] or W > F substitutants[46]. Peptides from noncoding ORFs were generated using *callNovelORF* with ORF order as min and with or without alternative translation. Noncoding ORF peptide databases were also generated for each alternative protease used in processing of the tonsil proteome, with appropriate number of maximum miscleavages as outlined above.

Non-canonical peptide databases were generated for 376 CCLE cell lines, 375 of which have non-reference channel proteomics characterization. This included all 10 cell lines in the bridge line and 366 non-reference cell lines with mutation data. Of the 378 non-reference channels across 42 plexes, three cell lines were duplicated, seven were in the bridge line, two didn't have mutation or fusion information and additional eight didn't have fusion information. Variant databases from all cell lines in a TMT plex, including the ten cell lines in the reference channel, were merged along with noncoding ORF peptides to generate plex-level databases. Plex-level databases were split into three tiers: 'Coding' (SNVs, indels and fusion in coding transcripts), 'Noncoding' (novel ORFs) and 'Noncoding Variant' (SNVs, indels and fusion in noncoding transcripts).

Non-canonical peptide databases for the proteome of mouse strain C57BL/6 N were generated by calling variant peptides based on germline SNPs and indels, followed by merging with the noncoding ORF peptides. The resulting non-canonical peptides were then split into 'Germline' (variants in coding transcripts), 'Noncoding' (novel ORFs) and 'Noncoding-Germline' (variants in noncoding transcripts).

For the eight ccRCC tumors, sample-specific variant peptides were called from germline/somatic SNVs and indels, RNA editing, transcript fusion and alternative splicing. Resulting peptides were merged with noncoding ORF and alternative translation peptides and split into four tiers: 'Variant' (variants in coding transcripts), 'Noncoding' (novel ORFs), 'Noncoding Variant' (variants in noncoding transcripts) and 'Alt Translation' (selenocysteine termination and W > F substitutants[46]).

For the five prostate tumors, variant peptides were called from all available genomic and transcriptomic variants, including germline/somatic SNVs and indels, RNA editing sites, transcript fusions, alternative splicing and circRNA. These peptides were then merged with the noncoding ORF and alternative translation peptides and split into five tiers: 'Variant' (variants in coding transcripts), 'Noncoding' (novel ORFs), 'Noncoding Variant' (variants in noncoding transcripts), 'Circular RNA' (circRNA ORFs) and 'Alt Translation' (selenocysteine termination and W > F substitutants[46]).

Non-canonical database search

Non-canonical database searches were performed similarly to canonical proteome searches for each dataset, as described in detail above. Custom databases of peptide sequences were concatenated with the reverse sequence for FDR control. Non-canonical peptide searches with Comet (v2019.01r5) were set to 'no cleavage' and did not permit protein N-terminus modifications or clipping of N-terminus methionine. Peptide-level FDR was set to 1% independently for each tier of non-canonical database, and PSMs of peptides that passed FDR were removed from the mzML for subsequent searches. Post hoc cohort-level FDR was calculated to verify an FDR cutoff smaller than 10% in tiers with at least 100 PSMs, as cohort-level FDR is not meaningful for smaller tiers. Each database tier thus had independent FDR control using database-specific decoy peptides, and a spectrum is excluded from subsequent searches after finding its most probable match. This strategy minimizes false-positives caused by joint FDR calculation with canonical peptides and enables a conservative detection of non-canonical peptides[7,18]. For CCLE, peptides were only considered for detection and quantitation for a cell line if they existed in the sample-specific database. For prostate tumors, additional searches were conducted with the same non-canonical databases using MSFragger (v3.3)[71] and X!Tandem (v2015.12.15)[72] with equivalent parameters for verification. For all datasets, quantified peptides were distinguished by charge and variable modifications, and detected but not quantified peptides were excluded from subsequent analysis.

DIA non-canonical spectral library search

Raw files were converted to.mzML files using ProteoWizard (3.0.21258)[65]. Sample-specific variant peptide FASTA databases were generated using the aforementioned non-canonical database generation pipeline, with individual spectral libraries.msp files generated by Prosit[42]. Prosit was configured with instrument type of LUMOS, collision energy of 34, and fragmentation method of HCD, with all default parameters otherwise. Searches were conducted using DIA-NN (v1.8.1)[44] against the sample-specific predicted variant peptide spectral libraries with protein inference disabled, a q-value cutoff of 0.01, and 'high precision' quantification.

Neoantigen prediction

Neoantigens were predicted from non-canonical peptides detected in CCLE proteomes. Cell line-specific *HLA* genotype was inferred using OptiType (v1.3.5)[73] from WGS or WXS data. Detected non-canonical peptides from the 'Coding' tier were converted to FASTA and analyzed using MHCflurry (v2.0.6)[74] with default parameters and cell line-specific *HLA* genotypes.

Statistical analysis and data visualization

All statistical analysis and data visualization were performed in the R statistical environment (v4.0.3), with visualization using BoutrosLab.plotting.general (v6.0.2)[75]. All boxplots, except for Extended Data Fig. 7a, show all data points, the median (center line), upper and lower quartiles (box limits), and whiskers extend to the minimum and maximum values within 1.5 times the interquartile range. In Extended Data Fig. 7a, data are summarized as boxplots to improve visual clarity without individual points due to the large number of gene and cell line combinations. All comparisons were performed on biological replicates, defined as independent patients, tumors, or cell lines as appropriate to each analysis. Schematics were created in Inkscape (v1.0) and Adobe Illustrator (27.8.1), and figures were assembled using Inkscape (v1.0).

Gene dependency association analysis. Gene dependency data from CCLE CRISPR screens were downloaded from the DepMap data portal (https://depmap.org/portal, 24Q2). Twelve cell lines with non-canonical peptide detections in proteomic data from at least ten genes were selected. The CERES scores[76] of genes with non-canonical peptide hits were compared to those without, using the Mann-Whitney U-test. Additionally, pooled CERES scores across all genes and cell lines were compared between the two groups using the same test. For *KRAS*, CERES scores and RNA abundance were compared between cell lines with non-canonical peptide detections in proteomic data and those with only canonical peptides, using the Mann-Whitney *U*-test.

Spectrum visualization and validation. Target PSM experimental spectra were extracted from mzML files using pyOpenMS (v3.1.0)[77] and visualized in R. Theoretical spectra were generated from the target peptide sequences using the TheoreticalSpectrumGenerator module of OpenMS and compared to the experimental spectra using hyperscores via the HyperScore module with consistent parameters as described above (for example, fragment mass tolerance). Fragment ion matching between the experimental and theoretical spectra was performed using a similar approach to IPSA[78]. Theoretical spectra with predicted fragment peak intensities were generated using Prosit via Oktoberfest (v0.6.2)[79] with parameters (for example, fragmentation method and energy) matching the original publication[41] and compared using cross-correlation[80] with settings matching Comet searches (for example, fragment_bin_offset). To assess the distribution of cross-correlation values for variant peptide PSMs, we randomly selected 1,000 canonical PSMs from each of the 42 TMT-plexes as control. circRNA peptide PSMs were validated using the Novor algorithm through app.novor.cloud, using parameters (for example, fragmentation method, MS2 analyzer, enzyme, precursor and fragment mass tolerance) consistent with database searches[45].

Cohort-level FDR. A post hoc approach was used to estimate the FDR threshold at the cohort level for each database tier. Within each sample and database tier, we first identified the target hit with the highest FDR value under the 1% threshold, denoted as FDR_i:

$$\mathrm{FDR}_i = \max_{j\in\{1,2,\ldots,n\}} \left(\mathrm{FDR}_j | \mathrm{FDR}_j < 0.01\right)$$

The number of decoy and target hits with FDR values less than FDR_i for each sample was tallied. The equivalent cohort-level FDR threshold was then calculated by dividing the total number of decoy hits by the total number of target and decoy hits across the cohort:

$$\text{Cohort} - \text{level FDR cutoff} = \frac{\sum 1\left(\text{Decoy Hits FDR}_j \le \text{FDR}_i\right)}{\sum 1\left(\text{Target \& Decoy Hits FDR}_j \le \text{FDR}_i\right)}$$

Reporting summary

Further information on research design is available in the Nature Portfolio Reporting Summary linked to this article.

Data availability

Data supporting the conclusions of this paper are included within it and its Supplementary Information. The processed CCLE data are available at the DepMap portal (http://www.depmap.org). The raw WGS and WXS cell lines sequencing data are available at Sequence Read Archive (SRA) and European Genome-Phenome Archive (EGA) under access numbers PRJNA523380 (ref. 40) and EGAD00001001039 (ref. 81). The raw mass spectrometry proteomic data are publicly available without restrictions at the ProteomeXchange via the PRIDE partner repository under accession numbers PXD030304 (ref. 41) for cell lines, PXD030983 (ref. 37) for mouse strain C57BL/6 N and PXD010154 (ref. 38) for alternative protease and fragmentation analyses. The proteomic data for the five prostate tumor samples are freely available at UCSD's MassIVE database under accession number MSV000081552 (ref. 36), whereas their raw WGS and RNA-seq data are available at EGA under accession EGAS00001000900 (ref. 35). Proteomic data for the eight ccRCC tumor samples are freely available at PDC under accession number PDC000411 (ref. 43), whereas the genomic and transcriptomic data are available at Genomic Data Commons (GDC, Project: CPTAC-3, Primary Site: Kidney) with dbGaP accession number phs001287, generated by the National Cancer Institute's Clinical Proteomic Tumor Analysis Consortium (CPTAC).

Code availability

moPepGen is publicly available at https://github.com/uclahs-cds/package-moPepGen (ref. 82). Data processing, analysis and visualization scripts are available upon request.

References

47. Cunningham, F. et al. Ensembl 2022. *Nucleic Acids Res.* **50**, D988–D995 (2022).
48. Zhu, C., Liu, L. Y., Kislinger, T. & Boutros, P. C. call-NonCanonicalPeptide: nextflow pipeline to generate custom databases of non-canonical peptides for proteogenomic analysis, Source code. https://github.com/uclahs-cds/pipeline-call-NonCanonicalPeptide (2025).
49. Di Tommaso, P. et al. Nextflow enables reproducible computational workflows. *Nat. Biotechnol.* **35**, 316–319 (2017).
50. Patel, Y. et al. NFTest: automated testing of Nextflow pipelines. *Bioinformatics* **40**, btae081 (2024).
51. Patel, Y., et al. Metapipeline-DNA: A Comprehensive Germline & Somatic Genomics Nextflow Pipeline. *bioRxiv* 2024.09.04.611267 https://doi.org/10.1101/2024.09.04.611267 (2024).
52. Zhao, H. et al. CrossMap: a versatile tool for coordinate conversion between genome assemblies. *Bioinformatics* **30**, 1006–1007 (2014).
53. McLaren, W. et al. The Ensembl Variant Effect Predictor. *Genome Biol.* **17**, 122 (2016).
54. Frankish, A. et al. GENCODE 2021. *Nucleic Acids Res.* **49**, D916–D923 (2021).
55. Danecek, P. et al. Twelve years of SAMtools and BCFtools. *Gigascience* **10**, giab008 (2021).
56. Vasimuddin, Md., Misra, S., Li, H. & Aluru, S. Efficient architecture-aware acceleration of BWA-MEM for multicore systems. In *2019 IEEE International Parallel and Distributed Processing Symposium (IPDPS)*; 314–324 (IEEE, 2019).
57. Poplin, R. et al. Scaling accurate genetic variant discovery to tens of thousands of samples. Preprint at *bioRxiv* https://doi.org/10.1101/201178 (2018).
58. DePristo, M. A. et al. A framework for variation discovery and genotyping using next-generation DNA sequencing data. *Nat. Genet.* **43**, 491–498 (2011).
59. Dobin, A. et al. STAR: ultrafast universal RNA-seq aligner. *Bioinformatics* **29**, 15–21 (2013).
60. Haas, B. J. et al. Accuracy assessment of fusion transcript detection via read-mapping and de novo fusion transcript assembly-based methods. *Genome Biol.* **20**, 213 (2019).
61. Shen, S. et al. rMATS: robust and flexible detection of differential alternative splicing from replicate RNA-seq data. *Proc. Natl Acad. Sci. USA* **111**, E5593–E5601 (2014).
62. Lo Giudice, C., Tangaro, M. A., Pesole, G. & Picardi, E. Investigating RNA editing in deep transcriptome datasets with REDItools and REDIportal. *Nat. Protoc.* **15**, 1098–1131 (2020).
63. Danecek, P. et al. The variant call format and VCFtools. *Bioinformatics* **27**, 2156–2158 (2011).
64. Zhang, X. O. et al. Diverse alternative back-splicing and alternative splicing landscape of circular RNAs. *Genome Res.* **26**, 1277–1287 (2016).

65. Chambers, M. C. et al. A cross-platform toolkit for mass spectrometry and proteomics. *Nat. Biotechnol.* **30**, 918–920 (2012).
66. Mellacheruvu, D. et al. The CRAPome: a contaminant repository for affinity purification mass spectrometry data. *Nat. Methods* **10**, 730 (2013).
67. Eng, J. K., Jahan, T. A. & Hoopmann, M. R. Comet: an open-source MS/MS sequence database search tool. *Proteomics* **13**, 22–24 (2013).
68. Röst, H. L. et al. OpenMS: a flexible open-source software platform for mass spectrometry data analysis. *Nat. Methods* **13**, 741–748 (2016).
69. Weisser, H. & Choudhary, J. S. Targeted feature detection for data-dependent shotgun proteomics. *J. Proteome Res.* **16**, 2964–2974 (2017).
70. Berry, M. J., Harney, J. W., Ohama, T. & Lhatfield, D. Selenocysteine insertion or termination: factors affecting UGA codon fate and complementary anticodon:codon mutations. *Nucleic Acids Res.* **22**, 3753–3759 (1994).
71. Kong, A. T., Leprevost, F. V., Avtonomov, D. M., Mellacheruvu, D. & Nesvizhskii, A. I. MSFragger: ultrafast and comprehensive peptide identification in mass spectrometry-based proteomics. *Nat. Methods* **14**, 513–520 (2017).
72. Craig, R. & Beavis, R. C. TANDEM: matching proteins with tandem mass spectra. *Bioinformatics* **20**, 1466–1467 (2004).
73. Szolek, A. et al. OptiType: precision HLA typing from next-generation sequencing data. *Bioinformatics* **30**, 3310–3316 (2014).
74. O'Donnell, T. J., Rubinsteyn, A. & Laserson, U. MHCflurry 2.0: improved pan-allele prediction of MHC class I-presented peptides by incorporating antigen processing. *Cell Syst.* **11**, 42–48 (2020).
75. P'ng, C. et al. BPG: Seamless, automated and interactive visualization of scientific data. *BMC Bioinformatics* **20**, 42 (2019).
76. Meyers, R. M. et al. Computational correction of copy number effect improves specificity of CRISPR-Cas9 essentiality screens in cancer cells. *Nat. Genet.* **49**, 1779–1784 (2017).
77. Röst, H. L., Schmitt, U., Aebersold, R. & Malmström, L. pyOpenMS: a Python-based interface to the OpenMS mass-spectrometry algorithm library. *Proteomics* **14**, 74–77 (2014).
78. Brademan, D. R., Riley, N. M., Kwiecien, N. W. & Coon, J. J. Interactive peptide spectral annotator: a versatile web-based tool for proteomic applications. *Mol. Cell Proteomics* **18**, S193–S201 (2019).
79. Picciani, M. et al. Oktoberfest: Open-source spectral library generation and rescoring pipeline based on Prosit. *Proteomics* **24**, 2300112 (2023).
80. Eng, J. K., Fischer, B., Grossmann, J. & MacCoss, M. J. A fast SEQUEST cross correlation algorithm. *J. Proteome Res.* **7**, 4598–4602 (2008).
81. Iorio, F. et al. A landscape of pharmacogenomic interactions in cancer. *Cell* **166**, 740–754 (2016).
82. Zhu, C., Liu, L. Y., Kislinger, T. & Boutros, P. C. moPepGen: multi-omics peptide generator. *GitHub* https://github.com/uclahs-cds/package-moPepGen (2025).

Acknowledgements

We thank members of the Boutros and Kislinger labs for their continued support, particularly A. Khoo, M. Govindarajan and M. Waas. We also thank J. Wohlschlegel from UCLA Proteome Research Center and M. Wilhelm from Technical University of Munich. This work was supported by the National Institutes of Health (NIH) via awards P30CA016042, U01CA214194, U2CCA271894, U24CA248265, P50CA092131 and R01CA244729; by the Canadian Cancer Society via an Impact Grant (705649); and by the Canadian Institute of Health Research via a Project Grant (PJT156357). C.Z. was supported by the UCLA Jonsson Comprehensive Cancer Center Fellowship Award. L.Y.L. was supported by a CIHR Vanier Fellowship and Ontario Graduate Scholarship. H.Z. was supported by a CIHR Doctoral Award. T.K. is supported through the Canadian Research Chair program. University Health Network was supported by the Ontario Ministry of Health and Long-Term Care.

Author contributions

Conceptualization was carried out by C.Z., L.Y.L., T.K. and P.C.B. Software development was performed by C.Z. and L.Y.L. Formal analysis was conducted by C.Z., L.Y.L., A.H., T.N.Y., H.Z., R.H.-W., J.L. and Y.P. Data curation was managed by C.Z., L.Y.L., A.H., T.N.Y., H.Z., R.H.-W., J.L. and Y.P. Visualization was completed by C.Z., L.Y.L. and A.H. The original draft of the manuscript was written by C.Z., L.Y.L., T.K. and P.C.B. All authors contributed to the review and editing of the manuscript.

Competing interests

P.C.B. sits on the scientific advisory boards of Intersect Diagnostics and previously sat on those of Sage Bionetworks and BioSymetrics. The other authors declare no competing interests.

Additional information

Extended data is available for this paper at https://doi.org/10.1038/s41587-025-02701-0.

Supplementary information The online version contains supplementary material available at https://doi.org/10.1038/s41587-025-02701-0.

Correspondence and requests for materials should be addressed to Chenghao Zhu, Thomas Kislinger or Paul C. Boutros.

Peer review information *Nature Biotechnology* thanks Pavel Sinitcyn and the other, anonymous, reviewer(s) for their contribution to the peer review of this work.

https://doi.org/10.1038/s41587-025-02701-0

Extended Data Table 1 | Feature comparison of custom database generation algorithms

Algorithm / Feature	moPepGen	customProDBJ[16–18]	MaxQuant module[19]	ProteoDisco[20]	ProteomeGenerator2[31,33]	pypgatk[21]	pyQUILTS[22]	samplespecificDBGenerator[23–25]	sapFinder / PGA[26,27]	spliceDB[28,29]	Spritz[30]	NeoDisc[32]
DNA Single Nucleotide Variants	✓	✓	✓	✓	✓	✓	✓	✓	✓	✓	✓	✓
DNA Small Insertions / Deletions	✓	✓		✓	✓	✓	✓		✓	✓	✓	✓
RNA Point Variants[a]	✓										✓	
Alternative Splice Junctions	✓			✓	✓		✓	✓	✓	✓		
Fusion Transcripts	✓			✓	✓		✓	✓	✓	✓		
Circular RNAs	✓											
Supported Variant Combinations	Any combi-nations[b]	None	All SNVs only[c]	All SNVs only[c]	All variants only[c]	None	Single SNV with splicing or fusion[d]	None	None	All variants only[c]	None	All variants only[c]
Modular Support for New Input Formats	✓							✓				
Noncoding Transcript Three-Frame Translation	✓				✓	✓			✓			✓
Noncoding Transcript with Variants[e]	✓				✓							✓
Alternative Translation W>F[f]	✓											
Export Only Non-canonical Proteotypic Peptides	✓			✓				✓	✓			
Summary of Database Generation	✓	✓			✓				✓			✓
Visualization of Database Generation	✓								✓			✓
Database Splitting for Tiered False Discovery Rate Control	✓											
Filter FASTA by RNA Abundance	✓				✓			✓				✓

[a]RNA Point Variants: variants at single-nucleotide positions within RNA sequences (for example, RNA editing). [b]Any variant combinations: generates peptides with any combination of variants. [c]All SNVs only / All variants only: generates peptides containing all variants simultaneously, but not separate combinations of individual variants. [d]Single SNV with splicing or fusion: generates peptides with a single SNV, with or without additional alternative splicing or transcript fusion events. [e]Noncoding Transcript with Variants: non-canonical peptides derived from novel open reading frames in noncoding transcripts harboring additional DNA and/or RNA variants. [f]W>F: tryptophan-to-phenylalanine substitutants[46]

https://doi.org/10.1038/s41587-025-02701-0

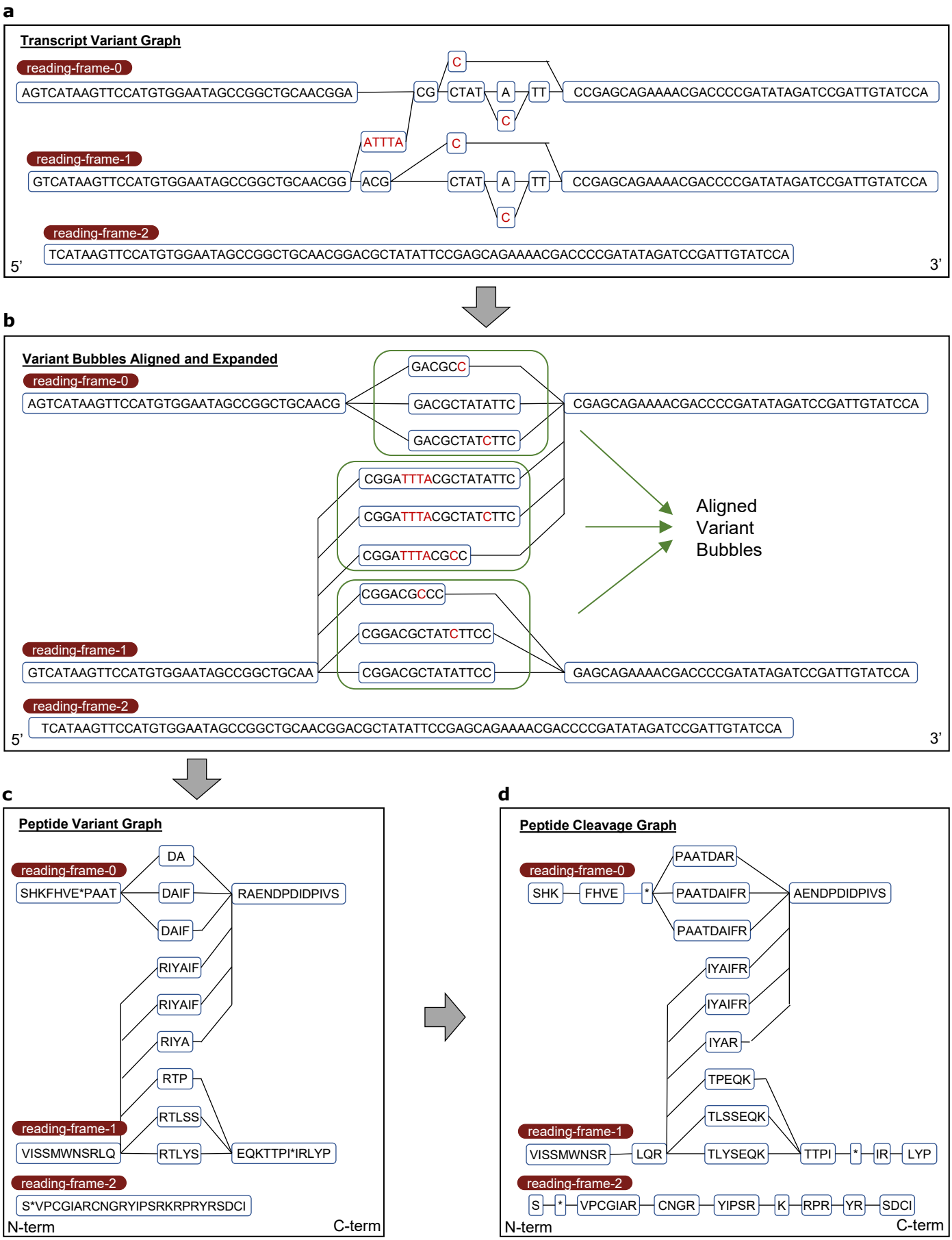

Extended Data Fig. 1 | See next page for caption.

https://doi.org/10.1038/s41587-025-02701-0

Extended Data Fig. 1 | Core graph algorithm of moPepGen. The graph algorithm of moPepGen implements the following key steps: **a**) A transcript variant graph (TVG) is generated from the transcript sequence with all associated variants. All three reading frames are explicitly generated to efficiently handle frameshift variants. **b**) Variant bubbles of the TVG are aligned and expanded to ensure the sequence length of each node is a multiple of three. **c**) Peptide variant graph (PVG) is generated by translating the sequence of each node of the TVG. **d**) Peptide cleavage graph is generated from the PVG in such a way that each node is an enzymatically cleaved peptide.

https://doi.org/10.1038/s41587-025-02701-0

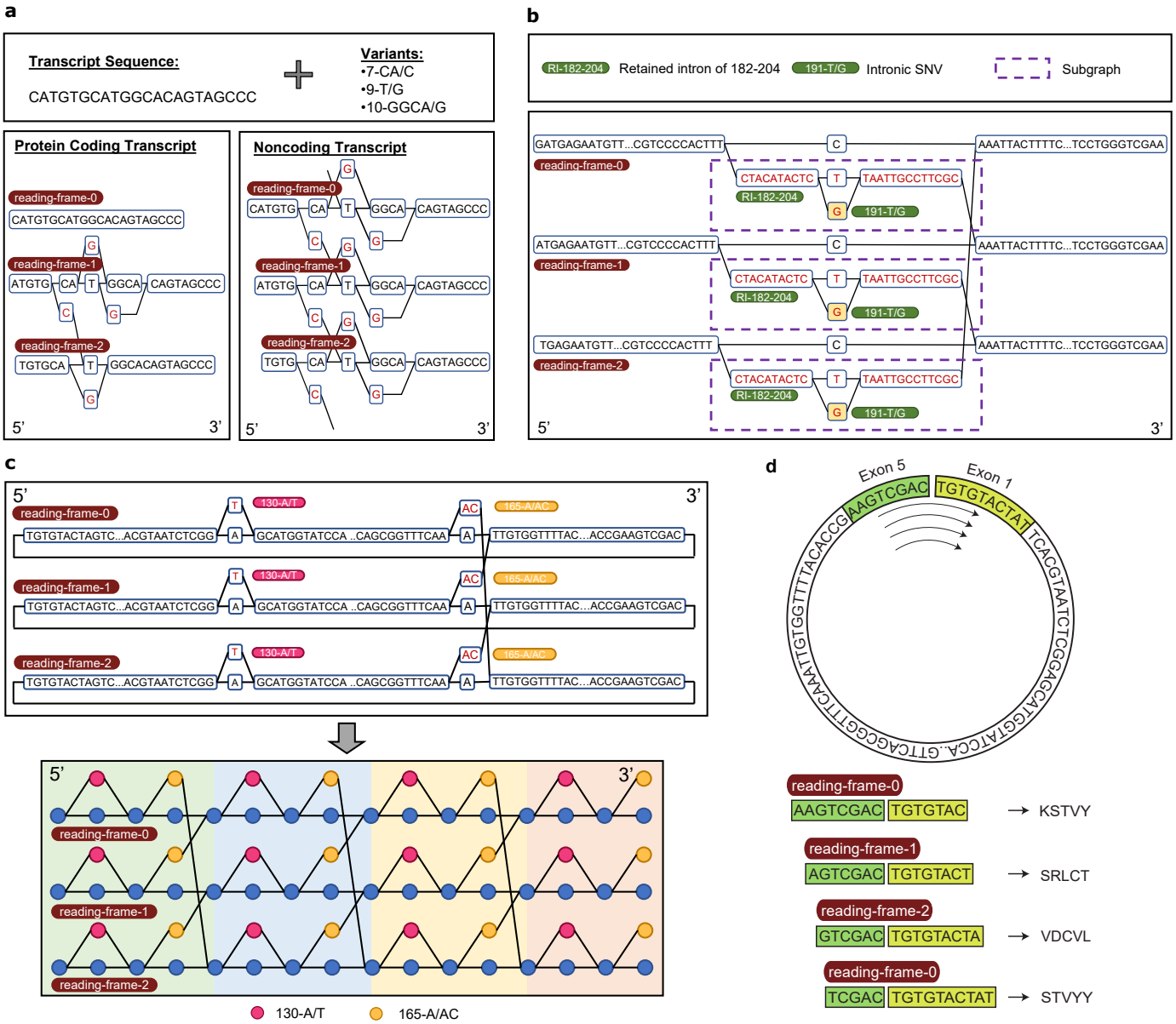

Extended Data Fig. 2 | Differential handling of noncoding transcripts, subgraphs and circular RNAs. a) For coding transcripts, variants are only incorporated into the effective reading frames. For transcripts that are canonically annotated as noncoding, variants are added to all three reading frames to perform comprehensive three-frame translation. **b**) Subgraphs are created for variant types that involve the insertion of large segments of the genome, which can carry additional variants. **c**) The graph of a circular RNA is extended four times to capture all possible peptides that span the back-splicing junction site in all three reading frames. In the bottom panel, the nodes in magenta harbor the variant 130-A/T and the nodes in yellow harbor 165-A/AC. **d**) Illustration of a circRNA molecule with a novel open reading frame. Each translation across the back-splicing site may shift the reading frame. If no stop codon is encountered, the original reading frame is restored after the fourth crossing.

https://doi.org/10.1038/s41587-025-02701-0

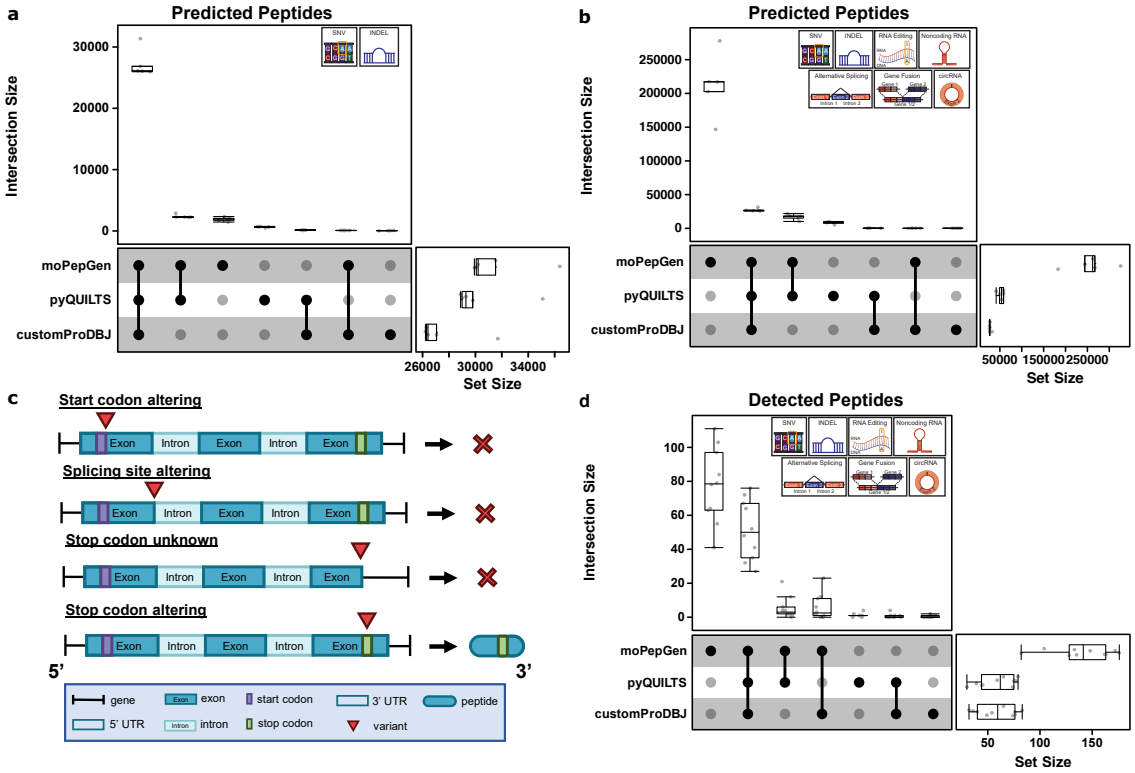

Extended Data Fig. 3 | moPepGen demonstrates comprehensive results and deliberate biological assumptions. a) and **b**) Non-canonical peptide generation results from benchmarking of moPepGen, pyQUILTS and customProDBJ using only point mutations (SNVs) and small insertions and deletions (indels; **a**), and with inputs from point mutations, indels, RNA editing, transcript fusion, alternative splicing and circular RNAs (circRNAs). **b**). Top boxplot shows the number of peptides in each set intersection and right barplot shows the total number of non-canonical peptides generated by each algorithm in five primary prostate tumour samples (n = 5). **c**) Assumptions made by moPepGen for handling edge cases that differ from other algorithms. Start-codon-altering and splice-site-altering variants are omitted due to the uncertainty of the resulting translation and splicing outcomes. Transcripts with unknown stop codons do not have trailing peptide outputs because of the uncertainty of the trailing enzymatic cleavage site. Stop-codon-altering variants do not result in translation beyond the transcript end, adhering to central dogma. UTR: untranslated region. **d**) Non-canonical database search results from benchmarking of moPepGen, pyQUILTS and customProDBJ using point mutations, indels, RNA editing, transcript fusion, alternative splicing and circRNAs (n = 5). All boxplots show the first quartile, median, to the third quartile, with whiskers extending to furthest points within 1.5× the interquartile range.

https://doi.org/10.1038/s41587-025-02701-0

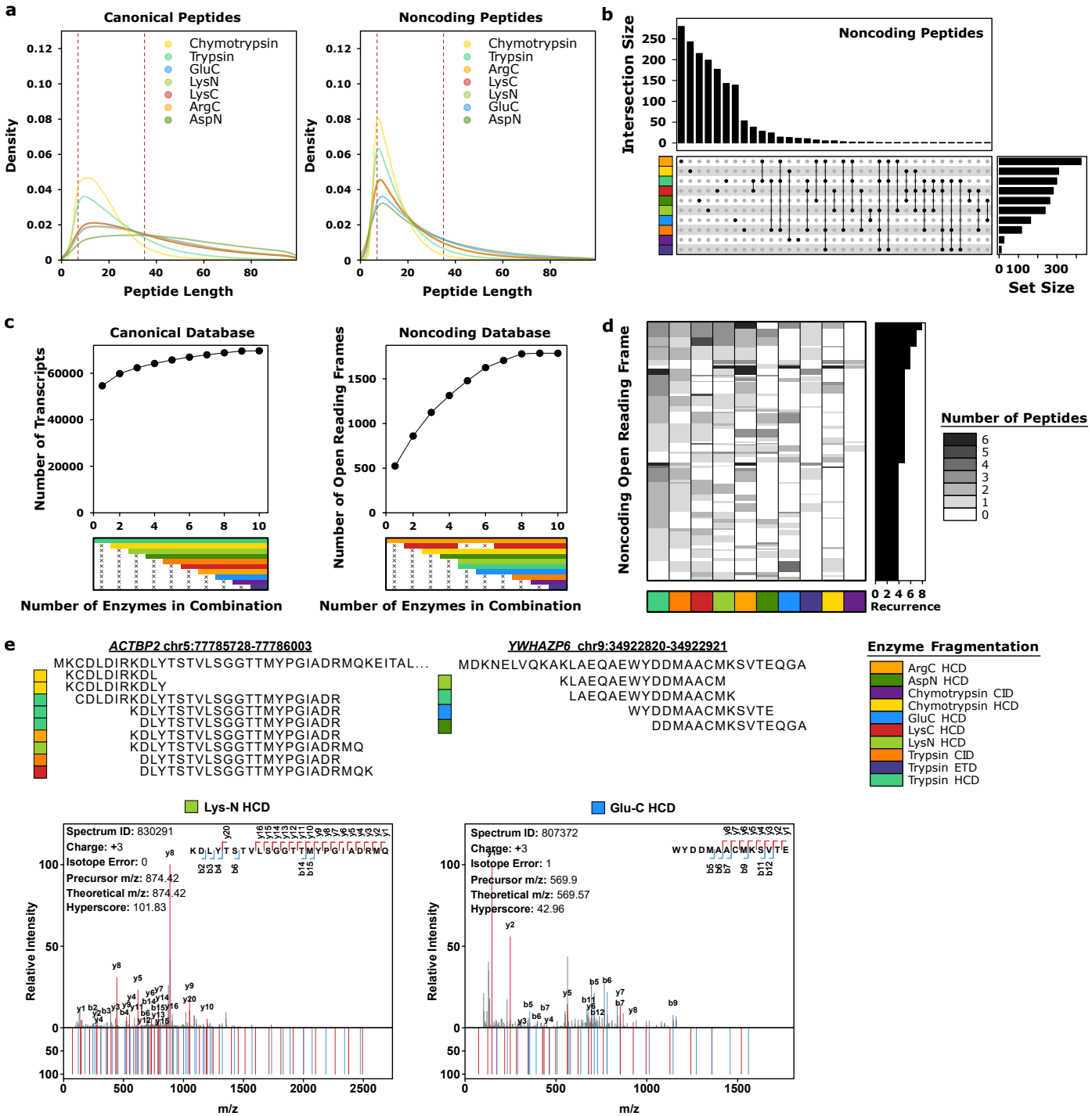

Extended Data Fig. 4 | Detection of novel open reading frame peptides across proteases. a) Peptide length distributions after *in silico* digestion with seven enzymes, as indicated by color, of the canonical human proteome and three-frame translated noncoding transcript open reading frames (ORFs). The dotted lines indicate the 7-35 amino acids peptide length range commonly used for database search. **b**) Noncoding peptide detection across ten enzyme-fragmentation methods in one deeply fractionated human tonsil sample. The top barplot shows the number of peptides in each set intersection and the right barplot shows the total number of non-canonical peptides from noncoding ORFs detected in each enzyme-fragmentation method, as indicated by covariate color. **c**) Optimal combinations of one to ten enzyme-fragmentation methods for maximizing the number of transcripts detected from the canonical proteome, or the number of ORFs detected from noncoding transcripts. The bottom covariate indicates the optimal combinations of enzyme-fragmentation methods from combinations of one to ten, with color indicating enzyme-fragmentation method. **d**) Noncoding transcript ORFs with peptides detected across four or more enzyme-fragmentation methods, with recurrence count shown in the right barplot. The color of the heatmap indicates the number of peptides detected per ORF per enzyme-fragmentation method. **e**) Example ORFs with coverage by multiple proteases are shown, with peptides tiled according to detection in each enzyme-fragmentation method, as indicated by covariate color. Representative fragment ion mass spectra of peptide-spectrum matches are shown, with theoretical spectra at the bottom and fragment ion matches colored (blue: b-ions, red: y-ions in). HCD: higher-energy collisional dissociation; CID: collision-induced dissociation; ETD: electron-transfer dissociation; *m/z*: mass-to-charge ratio.

https://doi.org/10.1038/s41587-025-02701-0

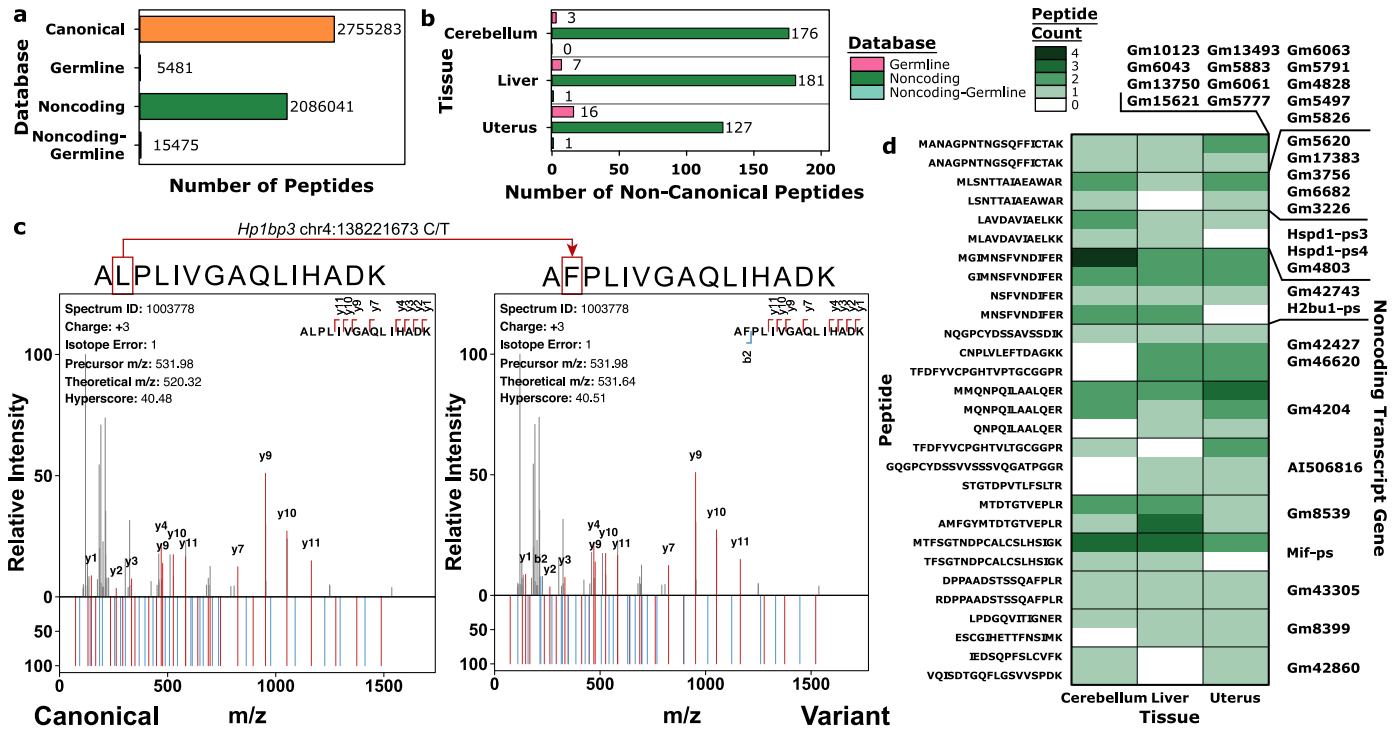

Extended Data Fig. 5 | Germline non-canonical peptide detection in mouse strain C57BL/6 N. a) Comparison of canonical and custom database sizes for the C57NL/6 N mouse. Germline database includes single-nucleotide polymorphisms (SNPs) and small insertions and deletions. **b**) Number of non-canonical peptides detected from each database in each tissue (one sample per tissue), with database indicated by color. **c**) Comparison of a variant peptide-spectrum match (PSM) spectra (top, both) with the theoretical spectra of the canonical peptide counterpart (left, bottom) as well as the theoretical spectra of the variant peptide harboring a SNP (right, bottom). Fragment ion matches are colored, with b-ions in blue and y-ions in red. *m/z*: mass-to-charge ratio. **d**) Noncoding transcripts with open reading frames yielding two or more non-canonical peptides recurrently detected across tissues, with color indicating the number of peptides detected in each tissue.

https://doi.org/10.1038/s41587-025-02701-0

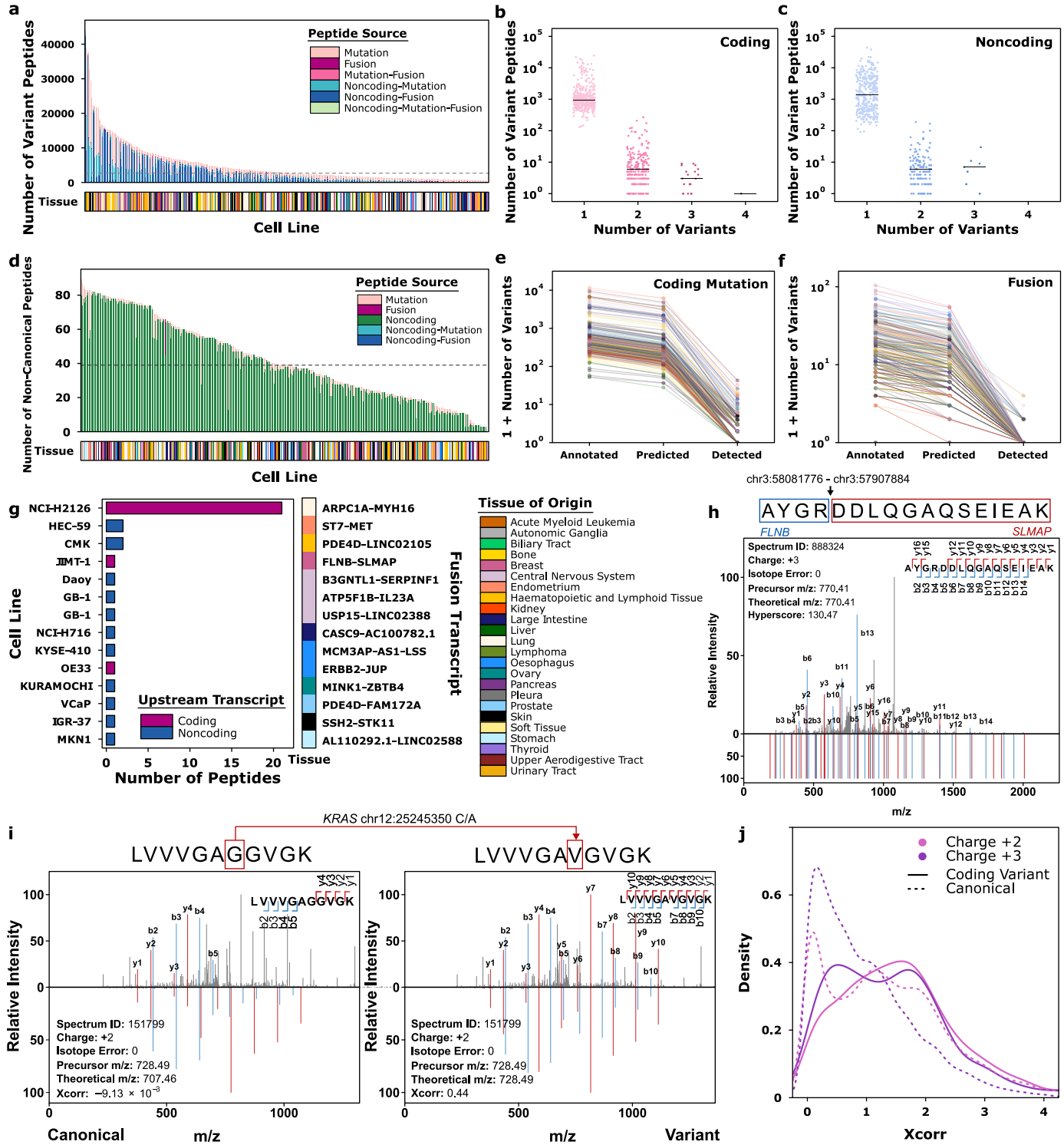

Extended Data Fig. 6 | See next page for caption.

https://doi.org/10.1038/s41587-025-02701-0

Extended Data Fig. 6 | Proteogenomic investigation of the Cancer Cell Line Encyclopedia. a) Number of non-canonical peptides generated per cell line, with color indicating peptide source. Bottom covariate indicates tissue of origin. **b**) and **c**) Number of variant peptides per cell line (n = 376) grouped by number of variants in combination in coding (**b**) and noncoding (**c**) transcripts. Lines indicate group median. **d**) Number of non-canonical peptides detected per cell line, colored by peptide source. Bottom covariate indicates tissue of origin. **e**) Per cell line, number of intragenic coding mutations (by VEP), mutations predicted to produce detectable non-canonical peptides and mutations detected through proteomics. **f**) Per cell line, number of transcript fusions, those predicted to produce detectable non-canonical peptides and fusions with detected peptide products. Color indicates tissue of origin. **g**) Fusion transcripts (upstream-downstream gene symbol) with detected peptides, with number of peptides shown across cell lines. Bar color indicates whether the upstream fusion transcript was coding or noncoding. Right covariate indicates tissue of origin. **h**) Fragment ion mass spectrum from peptide-spectrum match (PSM) of the non-canonical peptide at the junction of the *FLNB-SLMAP* fusion transcript. The peptide theoretical spectrum is shown at the bottom and fragment ion matches are colored (blue: b-ions, red: y-ions). **i**) Comparison of mass spectrum (top, both) from PSM of a non-canonical peptide with a single-nucleotide variant against Prosit-predicted MS2 mass spectra based on the canonical counterpart peptide sequence (left, bottom) and the detected variant peptide sequence (right, bottom). Fragment ion matches are colored, with b-ions in blue and y-ions in red. **j**) Cross-correlation (Xcorr) distribution of coding variant peptides PSMs against Prosit-predicted fragment mass spectra (solid lines, color indicate charge), in comparison with Xcorr of control canonical PSMs against Prosit-predicted mass spectra (dotted lines). *m/z*: mass-to-charge ratio.

https://doi.org/10.1038/s41587-025-02701-0

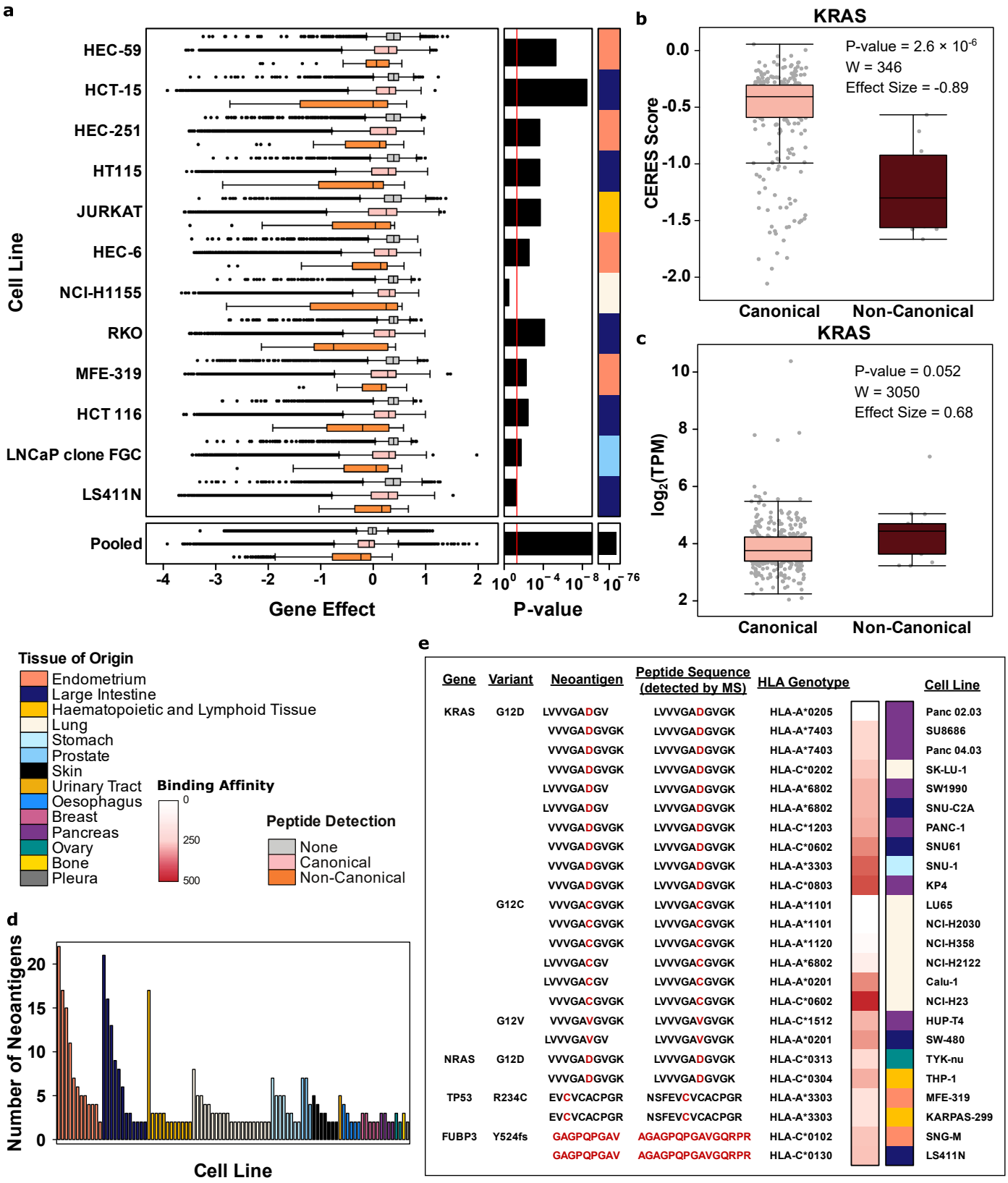

Extended Data Fig. 7 | See next page for caption.

https://doi.org/10.1038/s41587-025-02701-0

Extended Data Fig. 7 | Functional investigation of non-canonical peptide detection in Cancer Cell Line Encyclopedia. a) Gene effect CERES scores for genes with detected non-canonical peptides (orange), detected canonical peptides only (pink) and no detected peptides (gray). A lower CERES score indicates higher gene dependency. Cell lines were selected based on the detection of non-canonical peptides in more than 10 genes. P-values were calculated using a two-sided Mann-Whitney U-test. The red vertical line indicates $\alpha = 0.05$. The bottom panel represents data pooled across all genes and cell lines. The number of genes per group per cell line and Mann-Whitney U-test results are provided in Supplementary Table 9. **b**) Gene effect CERES score and **c**) mRNA abundance of *KRAS* in cell lines with only canonical peptides detected compared to those with detected non-canonical peptides (n = 290 and 12, respectively). P-values were calculated using a two-sided Mann-Whitney U-test. TPM: Transcript per million. **d**) Number of putative neoantigens predicted based on detected non-canonical peptides in cell lines with more than two neoantigens. The color indicates cell line tissue of origin. **e**) Recurrent neoantigens observed across multiple cell lines, along with their associated gene, variant, *HLA* genotype and the full peptide sequence as detected by trypsin-digested whole cell lysate mass spectrometry. The color in the left heatmap represents neoantigen binding affinity. Right covariate indicates tissue of origin. All boxplots show the first quartile, median, to the third quartile, with whiskers extending to furthest points within 1.5× the interquartile range.

https://doi.org/10.1038/s41587-025-02701-0

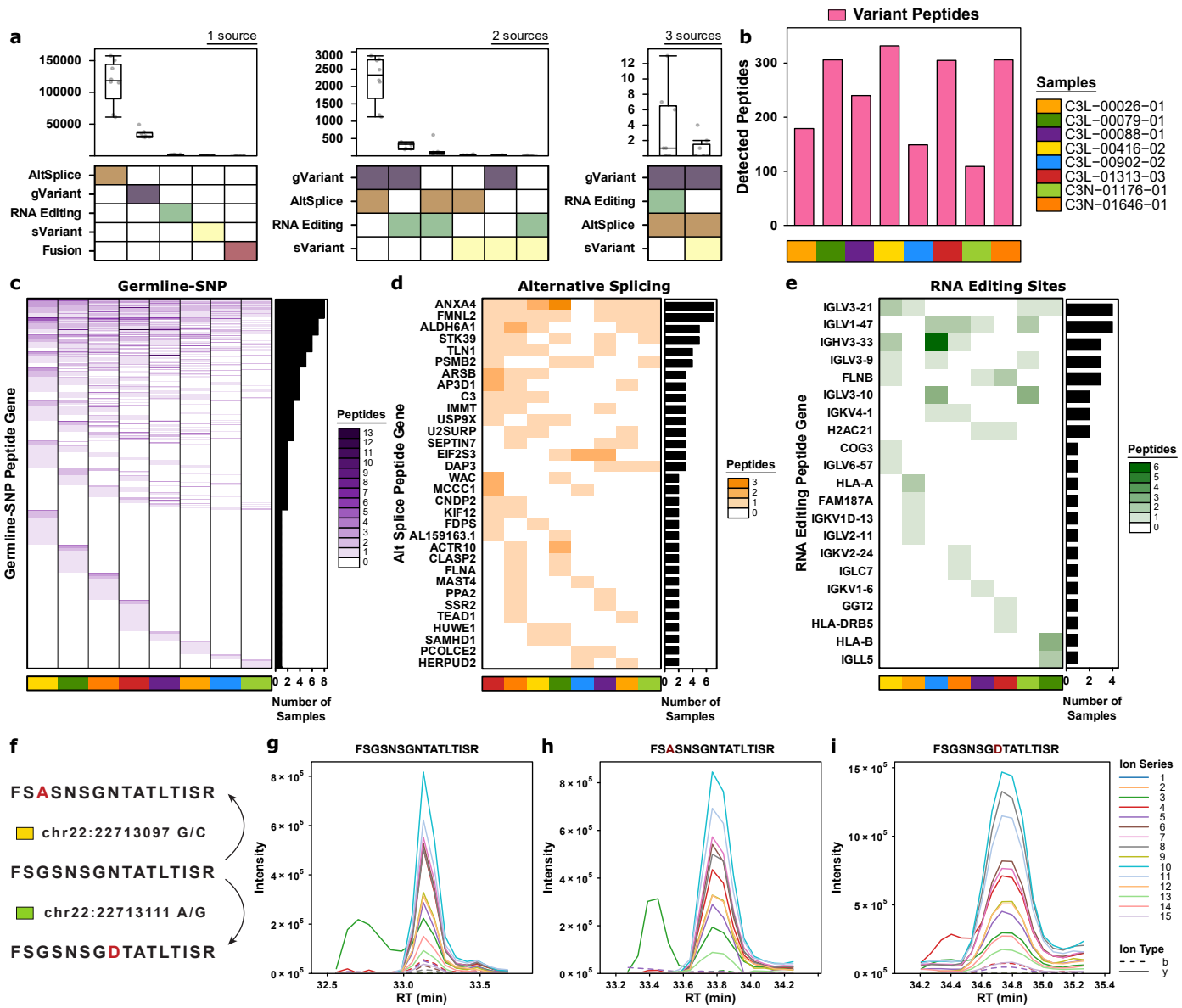

Extended Data Fig. 8 | Detection of non-canonical peptides from DIA proteomics. a) Number of variant peptides from different variant combinations generated using genomic and transcriptomic data from eight clear cell renal cell carcinoma (ccRCC) tumors (n = 8), grouped by the number of variant sources in combination. gVariant: germline single-nucleotide polymorphism and insertion/deletions (indels); sVariant: somatic single-nucleotide variant and indels; AltSplice: alternative splicing. **b**) Number of detected variant peptides in the data-independent acquisition (DIA) proteome of eight ccRCC tumors. **c**-**e**) Detection of non-canonical peptides harboring germline single-nucleotide polymorphisms (**c**), alternative splicing (**d**) and RNA editing sites (**e**) across genes. Heatmap colors indicate the number of peptides detected per gene per sample. The barplot indicates recurrence across samples. **f**) Illustration of non-canonical peptides derived from the canonical sequence FSGSNSGNTATLTISR in gene *IGLV3-21* caused by RNA editing events. **g**-**i**) Extracted ion chromatograms of the canonical peptide (**g**) and non-canonical peptides derived from *IGLV3-21* caused by RNA editing events: chr22:22713097 G-to-C (**h**) and chr22:22713111 A-to-G (**i**). All boxplots show the first quartile, median, to the third quartile, with whiskers extending to furthest points within 1.5× the interquartile range.

https://doi.org/10.1038/s41587-025-02701-0

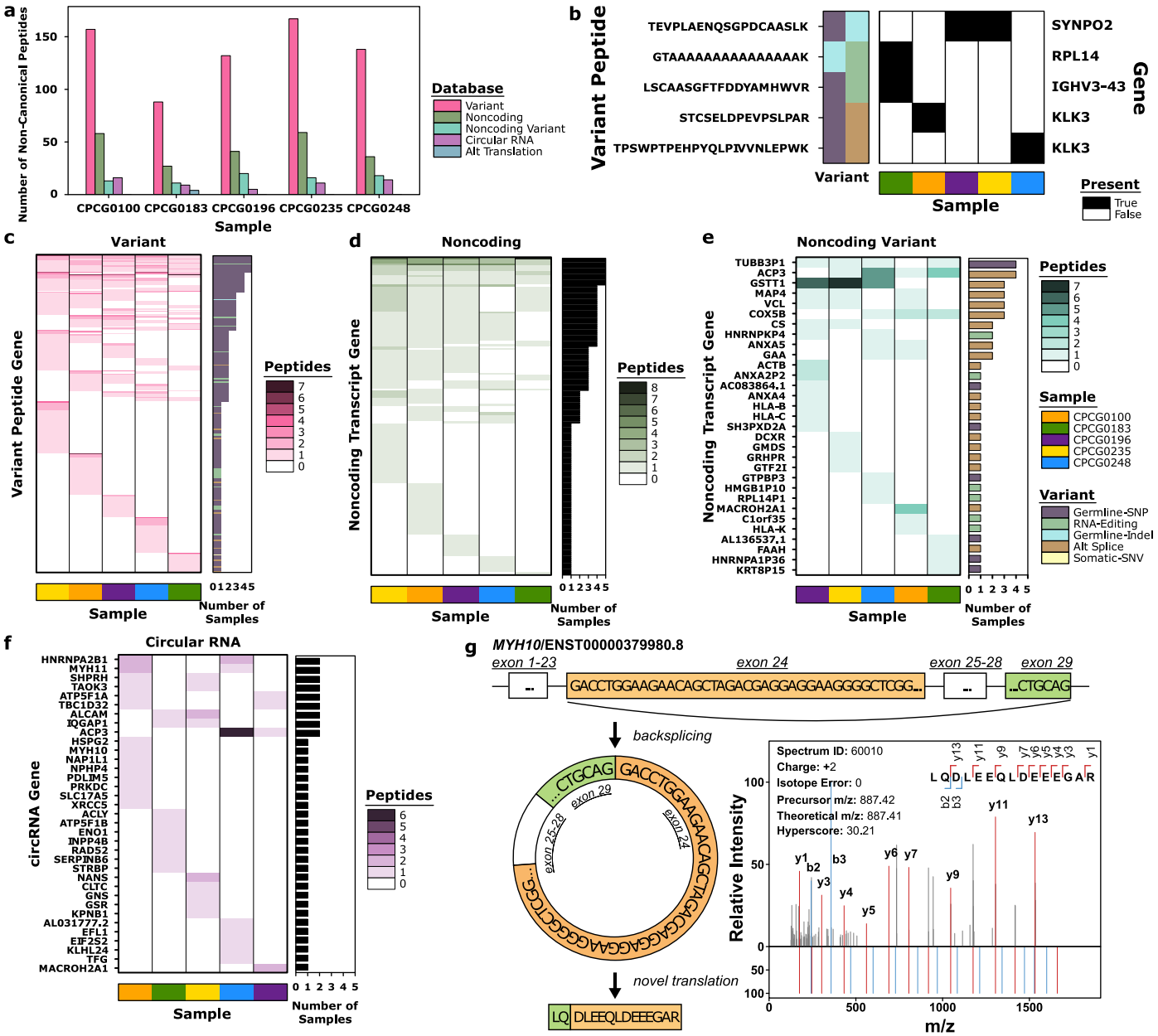

Extended Data Fig. 9 | Detection of non-canonical peptides from genomic variants, alternative splicing and circular RNAs. a) Number of detected non-canonical peptides in five primary prostate tumour samples per database tier (colored by database). **b**) Peptides as the result of a combination of two variants, with variant type indicated in left covariate and gene on the right. The heatmap shows presence of peptide across samples. **c**-**f**) Non-canonical peptide detection results across genes, with color of heatmap representing the number of peptides detected per gene per sample. The barplot indicates recurrence across samples, and when colored indicates variant type associated with the gene entry. The Variant database includes non-canonical peptides from coding transcripts with single-nucleotide polymorphisms (SNPs), single-nucleotide variants (SNVs), small insertion and deletion (indels), RNA editing, alternative splicing (Alt Splice) or transcript fusion (**c**). Noncoding database includes all peptides from noncoding transcript three-frame translation open reading frames (**d**) and noncoding peptides with any variants are included in the Noncoding Variant database (**e**). The Circular RNA database includes all peptides representing circular RNA open reading frames (ORFs) with or without other variants (**f**). The bottom covariate indicates prostate cancer sample. **g**) Mass spectrum from peptide-spectrum match of a non-canonical peptide spanning the back-splicing junction between exon 29 and exon 24 of *MYH10*, reflective of circular RNA translation. The peptide theoretical spectrum is shown at the bottom and fragment ion matches are colored (blue: b-ions, red: y-ions in). *m/z*: mass-to-charge ratio.

nature portfolio

Corresponding author(s): Chenghao Zhu
Thomas Kislinger
Paul C. Boutros

Last updated by author(s): May 7, 2025

Reporting Summary

Nature Portfolio wishes to improve the reproducibility of the work that we publish. This form provides structure for consistency and transparency in reporting. For further information on Nature Portfolio policies, see our Editorial Policies and the Editorial Policy Checklist.

Statistics

For all statistical analyses, confirm that the following items are present in the figure legend, table legend, main text, or Methods section.

n/a	Confirmed	
☐	☒	The exact sample size (*n*) for each experimental group/condition, given as a discrete number and unit of measurement
☐	☒	A statement on whether measurements were taken from distinct samples or whether the same sample was measured repeatedly
☐	☒	The statistical test(s) used AND whether they are one- or two-sided *Only common tests should be described solely by name; describe more complex techniques in the Methods section.*
☒	☐	A description of all covariates tested
☐	☒	A description of any assumptions or corrections, such as tests of normality and adjustment for multiple comparisons
☐	☒	A full description of the statistical parameters including central tendency (e.g. means) or other basic estimates (e.g. regression coefficient) AND variation (e.g. standard deviation) or associated estimates of uncertainty (e.g. confidence intervals)
☐	☒	For null hypothesis testing, the test statistic (e.g. *F*, *t*, *r*) with confidence intervals, effect sizes, degrees of freedom and *P* value noted *Give P values as exact values whenever suitable.*
☒	☐	For Bayesian analysis, information on the choice of priors and Markov chain Monte Carlo settings
☒	☐	For hierarchical and complex designs, identification of the appropriate level for tests and full reporting of outcomes
☒	☐	Estimates of effect sizes (e.g. Cohen's *d*, Pearson's *r*), indicating how they were calculated

Our web collection on statistics for biologists contains articles on many of the points above.

Software and code

Policy information about availability of computer code

Data collection	No software was used to download the data used in this publication.
Data analysis	• moPepGen is available on GitHub: https://github.com/uclahs-cds/package-moPepGen and PyPI: https://pypi.org/project/mopepgen (licensed under GPL-2.0) • The non-canonical peptide calling pipeline is available on GitHub: https://github.com/uclahs-cds/pipeline-call-NonCanonicalPeptide • The DNA processing metapipeline is available on GitHub: https://github.com/uclahs-cds/metapipeline-DNA and includes the following software: BWA-MEM2 (v2.2.1), Picard Tools (v2.27.4), GATK (v4.2.5.0 and v4.2.4.1), SAMtools (v1.15.1), MuTect2 (from GATK v4.5.0.0), VCFtools (v0.1.16), BCFtools (v1.9-1) and VEP (v104) • RNA-seq data were processed using: STAR (v2.7.10b), SAMtools (v1.15.1), STAR-Fusion (v1.9.1), rMATS (v4.1.1), REDItools2 (v1.0.0) and CIRCexplorer2 (v2.3.8) • Proteomics data were processed using: ProteoWizard MSConvert (3.0.21258), Comet (v2019.01r5), MSFragger (v3.3), X!Tandem (v2015.12.15), OpenMS (v3.0.0-1f903c0), DIA-NN (v1.8.1) and Novor (app.novor.cloud) • Neoantigens were predicted using OptiType (v1.3.5) and MHCflurry (v2.0.6) • PSM validation were done using pyOpenMS (v3.1.0) and Oktoberfest (v0.6.2) • Data analysis was performed using: R (v4.0.3), BoutrosLab.plotting.general (v6.0.2), data.table (v1.14.0), Python (v3.8.10)

For manuscripts utilizing custom algorithms or software that are central to the research but not yet described in published literature, software must be made available to editors and reviewers. We strongly encourage code deposition in a community repository (e.g. GitHub). See the Nature Portfolio guidelines for submitting code & software for further information.

Data

Policy information about availability of data

All manuscripts must include a data availability statement. This statement should provide the following information, where applicable:

- Accession codes, unique identifiers, or web links for publicly available datasets
- A description of any restrictions on data availability
- For clinical datasets or third party data, please ensure that the statement adheres to our policy

The processed CCLE data are available at the DepMap portal (http://www.depmap.org). The raw WGS and WXS cell lines sequencing data are available at Sequence Read Archive (SRA) and European Genome-Phenome Archive (EGA) under access number PRJNA52338041 and EGAD0000100103990. The raw mass spectrometry proteomic data are publicly available without restrictions at the ProteomeXchange via the PRIDE partner repository under accession number PXD03030442 for cell lines, PXD03098337 for mouse strain C57BL/6N, and PXD01015491 for alternative protease and fragmentation analyses. The proteomic data for the five prostate tumour samples are freely available at UCSD's MassIVE database under accession number MSV00008155236, whereas their raw WGS and RNA-seq data are available at EGA under accession EGAS0000100090035. Proteomic data for the eight kidney tumour samples are freely available at Proteomic Data Commons (PDC) under accession number PDC00041144, whereas the genomic and transcriptomic data are available at Genomic Data Commons (GDC, Project: CPTAC-3, Primary Site: Kidney) with dbGaP accession number phs001287, generated by the National Cancer Institute's Clinical Proteomic Tumor Analysis Consortium (CPTAC).

Research involving human participants, their data, or biological material

Policy information about studies with human participants or human data. See also policy information about sex, gender (identity/presentation), and sexual orientation and race, ethnicity and racism.

Reporting on sex and gender	This study did not involve human participants.
Reporting on race, ethnicity, or other socially relevant groupings	This study did not involve human participants.
Population characteristics	This study did not involve human participants.
Recruitment	This study did not involve human participants.
Ethics oversight	This study did not involve human participants.

Note that full information on the approval of the study protocol must also be provided in the manuscript.

Field-specific reporting

Please select the one below that is the best fit for your research. If you are not sure, read the appropriate sections before making your selection.

☒ Life sciences ☐ Behavioural & social sciences ☐ Ecological, evolutionary & environmental sciences

For a reference copy of the document with all sections, see nature.com/documents/nr-reporting-summary-flat.pdf

Life sciences study design

All studies must disclose on these points even when the disclosure is negative.

Sample size	The genomic and proteomic data for 375 cell lines were obtained from the Cancer Cell Line Encyclopedia project (Nusinow et al., 2020, Cell). Proteomic data for the three mouse tissue samples were obtained from Giansanti et al., 2022, Nat Methods. Proteomic data of a tonsil tissue sample, analyzed using 10 enzyme-fragmentation methods were accquired from Wang et al., 2019, Mol Syst Biol. The genomic and proteomic data for the 5 primary prostate tumours were obtained from Sinha et al., 2019, Cancer Cell. This study did not explicitly derive experimental groups, therefor the sample sizes were not determined based on statistical calculation.
Data exclusions	Data were included based on their accessibility. The 375 cancer cell lines were selected based on the availability of both proteomic and genomic data. The three mouse tissues (liver, uterus, and cerebellum) were chosen to cover the greatest tissue variability. Prostate tumors were selected because they have genomic and transcriptomic data available, as well as proteomic data from two injection replicates.
Replication	This study did not generate new experimental data from patients, samples, or cell lines. All analyses were performed using existing datasets and based on biological replicates, defined as independent patients, tumors, or cell lines, as appropriate to each analysis.
Randomization	As noted previously, this study did not explicitly derive experimental groups, and as such, no randomization was implemented during data analysis.
Blinding	Blinding was not employed during data analysis because this study involved secondary analysis of publicly available, pre-existing datasets. The goal of the analyses was to demonstrate the capability of moPepGen in detecting non-canonical peptides, and no conclusions were drawn from comparisons between predefined groups of samples.

Reporting for specific materials, systems and methods

We require information from authors about some types of materials, experimental systems and methods used in many studies. Here, indicate whether each material, system or method listed is relevant to your study. If you are not sure if a list item applies to your research, read the appropriate section before selecting a response.

Materials & experimental systems

n/a	Involved in the study
☒	☐ Antibodies
☒	☐ Eukaryotic cell lines
☒	☐ Palaeontology and archaeology
☒	☐ Animals and other organisms
☒	☐ Clinical data
☒	☐ Dual use research of concern
☒	☐ Plants

Methods

n/a	Involved in the study
☒	☐ ChIP-seq
☒	☐ Flow cytometry
☒	☐ MRI-based neuroimaging

Plants

Seed stocks	N/A
Novel plant genotypes	N/A
Authentication	N/A